ARRAY MEASUREMENTS OF P VELOCITIES IN THE LOWER MANTLE

By Lane R. Johnson*

ABSTRACT

The extended array at the Tonto Forest Seismological Observatory in central Arizona has been used to measure $dT/d\Delta$ of direct P waves from 212 earthquakes in the distance range between 30 and 100°, and these data have been inverted to obtain a velocity model for the lower mantle. Travel times calculated for this model are in good agreement with empirical travel times. The $dT/d\Delta$ data from different azimuths and from different focal depths are all in reasonably good agreement with the exception of anomalously large values from earthquakes on the mid-Atlantic ridge. The effect of the core on the measured values of $dT/d\Delta$ at distances greater than 90° is shown to be significant, and a correction is made for this effect. A curve fit to the $dT/d\Delta$ data contains anomalous regions near the epicentral distances of 34.5, 40.5, 49.5, 59.5, 70.5, and 81.5° which may correspond to increased velocity gradients near the depths of 830, 1000, 1230, 1540, 1910, and 2370 km. PcP times were used to estimate a core radius of 3481 km.

INTRODUCTION

The first attempts to determine the variation of elastic velocities in the Earth from the travel times of seismic waves took place during the first decade of this century. By 1939 the standard models of Gutenberg and Jeffreys had evolved. Later studies by Gutenberg and Jeffreys and studies using similar techniques have changed these models relatively little. If we consider the lower mantle, which we shall take to be roughly the region D of Bullen between the approximate depths of 900 and 2900 km, we find that the standard models of Gutenberg and Jeffreys are fairly similar. There is little doubt that either of these models represents a close approximation to the true velocities in the lower mantle, and thus any differences between these models and an improved velocity model will be relatively small.

The velocities of seismic body waves are the most direct measurements of physical properties in the lower mantle and as such have been used extensively to infer other physical properties such as elastic constants, density, and chemical composition (for example, Birch, 1952, 1961, 1964; Anderson, 1966; Bullen and Haddon, 1967). Because these velocities occupy such a fundamental position in our understanding of the lower mantle, any small improvements which we can make in their values are important and well worth the effort of obtaining them.

In the past most velocity models for the lower mantle have been derived from the measured travel times of the seismic waves generated by earthquakes. In the last decade the use of nuclear explosions as the source of the seismic waves has led to improved travel-time data for P waves because it eliminates many of the uncertainties associated with the source. Systematic methods of analyzing the travel time data which take account of station corrections have also helped increase the accuracy of the travel-time curves. While these travel-time curves are of great importance in their own right, they also can be used to obtain velocity models for the mantle. Recently

---

* Now at the Department of Geology and Geophysics, University of California, Berkeley.

Hales *et al.* (1968) and Ferrin *et al.* (1968a) have constructed average travel-time curves from analyses of both earthquakes and explosions and have inverted these travel-time curves to obtain velocity models for the mantle.

Large seismic arrays are a relatively new development in seismology but they have already contributed much to the study of velocities in the mantle. These arrays have the potential to yield more accurate velocity models because they allow a more direct measurement of the gradient of the travel time curve; this is the quantity which enters directly into the calculation of velocities. Niazi and Anderson (1965), Johnson (1966, 1967b), Chinnery and Toksöz (1967), and Kanamori (1967) have all used this method to investigate P velocities in the mantle.

In the present study we have used a large array to measure $dT/d\Delta$ of seismic body waves, and the resulting data have been inverted to obtain a velocity model for the
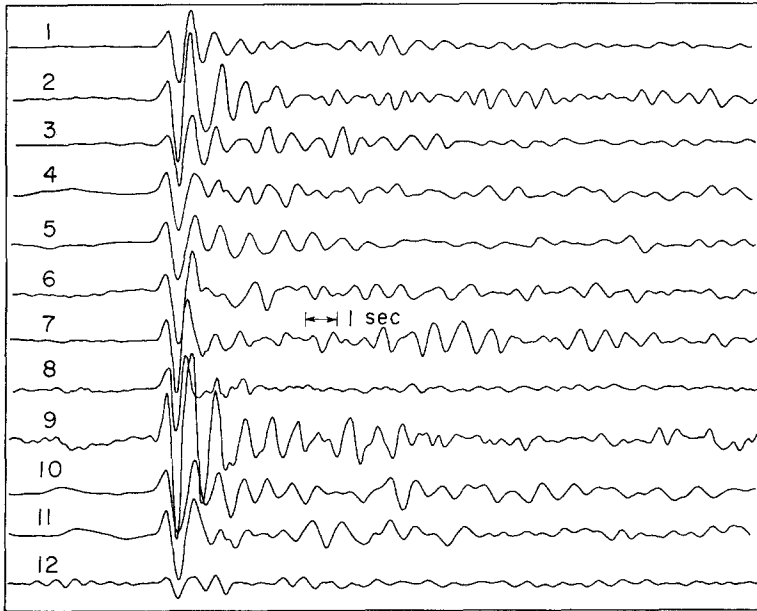

FIG. 1. Seismograms of the 12 array sites for an earthquake in the Chile-Bolivia region on 16 April 1965. (Depth = 127 km; magnitude = 5.0, distance = 69.6°, azimuth = 137°.) The various seismograms have been shifted in time so as to align the P wave on all of the seismograms.

mantle. This paper will be confined to results that were obtained from measurements of short-period compressional waves. Thus, unless explicitly stated otherwise, the term "velocity" will imply the velocity of short period (near 1 sec) compressional waves.

THE DATA

The basic data of the present study consist of the measured values of $dT/d\Delta$ (the gradient of the travel-time curve) of P waves from earthquakes. The measurements were made with the extended array at the Tonto Forest Seismological Observatory (TFSO or TFO) in central Arizona. The present study is actually a continuation of work reported in a previous paper (Johnson, 1967b) which dealt with the P velocities in the upper mantle. Descriptions of the array, the crustal structure underlying it, and the method by which $dT/d\Delta$ was measured can be found in that earlier paper, but for the sake of completeness we will briefly summarize those descriptions here.

The array consists of 12 elements arranged in two perpendicular legs with dimensions of 325 and 285 km short period vertical seismometers with a peak response

TABLE I

EARTHQUAKE DATA

No.	Date 1965	Location	Time		Δ deg	Azimuth deg	h km	Magni- tude	p sec/ deg	RMS Error sec
			h	m						
1	April 16	New Hebrides	09	59	93.0	248	62	5.0	4.56	.06
2	16	Chile-Bolivia	12	51	69.6	137	127	5.0	6.27	.09
3	16	Rat	14	33	53.2	311	38	5.0	7.34	.09
4	16	Argentina	22	54	77.4	143	151	4.6	5.72	.08
5	16	Alaska	23	22	42.1	331	5	5.8	8.14	.12
6	17	Near	00	00	55.3	314	43	5.1	7.18	.13
7	18	Panama	05	44	37.6	128	33	4.6	8.51	.16
8	18	S. Fiji	14	08	86.4	234	33	5.2	4.87	.08
9	20	Komandorsky	04	44	57.3	316	27	4.9	7.08	.10
10	20	Near	06	43	56.0	314	35	5.5	7.14	.14
11	20	Kamchatka	06	50	61.4	319	33	5.3	6.68	.05
12	20	Mariana	17	15	91.3	289	60	5.8	4.65	.14
13	22	New Hebrides	01	05	91.6	254	204	5.3	4.56	.09
14	22	Rat	18	36	53.6	313	37	5.1	7.34	.06
15	24	Kodiak	10	20	37.0	324	58	4.7	8.49	.15
16	24	Caribbean	13	25	34.2	122	33	4.4	8.66	.25
17	24	Near	20	12	56.4	315	25	5.1	7.14	.11
18	24	Caroline	21	55	98.7	290	59	5.7	4.41	.10
19	25	Kermadec	00	25	91.3	231	33	4.8	4.58	.10
20	25	Volcano	01	00	88.6	299	15	5.6	4.73	.09
21	25	Rat	01	43	52.1	312	49	5.2	7.38	.14
22	25	New Britain	06	52	98.8	270	49	5.4	4.54	.18
23	25	Bonin	14	05	87.9	302	53	5.2	4.78	.05
24	25	Ryukyu	21	28	93.6	310	28	4.9	4.56	.08
25	25	Alaska	01	57	32.2	330	33	5.3	8.89	.50
26	26	Tonga	13	32	80.3	238	33	4.9	5.46	.06
27	26	Alaska	20	29	40.9	316	53	5.9	8.19	.16
28	April 27	Rat	13	18	54.2	312	33	4.9	7.29	.10
29	27	Crete	14	09	98.6	36	50	5.5	4.58	.16
30	27	S. Pacific	15	06	70.1	173	33	4.7	6.23	.09
31	28	Andreanof	01	25	48.9	312	47	5.0	7.68	.07
32	28	Kermadec	10	26	86.8	234	33	5.4	4.82	.07
33	29	Chile	07	06	82.0	152	33	4.9	5.38	.08
34	29	Tonga	07	53	79.4	241	33	4.5	5.56	.08
35	29	S. Fiji	09	44	88.2	240	540	5.2	4.76	.07
36	29	Mariana	11	19	92.3	290	134	5.2	4.54	.10
37	30	Rat	16	00	54.3	313	33	5.1	7.29	.12
38	May 1	S. Alaska	01	58	34.3	330	13	4.6	8.68	.11
39	1	S. Mariana	13	02	95.2	289	5	5.1	4.45	.12
40	1	S. Alaska	21	27	34.4	330	33	5.3	8.68	.12
41	2	N. Chile	05	47	67.3	137	117	5.5	6.47	.19
42	2	Fiji	10	52	86.4	241	581	4.9	4.86	.11
43	3	Chile-Argen.	01	09	76.8	145	77	5.6	5.72	.10
44	3	Cen. America	01	17	39.8	134	33	4.9	8.36	.16
45	3	Chile-Argen.	16	09	71.7	138	114	5.6	6.12	.10
46	4	Peru	12	10	62.4	138	78	4.5	6.77	.14
47	5	N. Chile	03	00	67.7	137	96	4.6	6.42	.14
48	5	Peru	09	13	58.9	139	94	4.7	7.02	.16
49	5	Japan	21	33	75.9	312	33	4.9	5.73	.07
50	6	Chile-Argen.	02	25	71.9	139	90	5.1	6.07	.10
51	7	Mariana	02	29	93.0	289	57	4.9	4.54	.07
52	7	Japan	07	31	94.6	311	131	4.8	4.50	.10
53	7	Andreanof	22	44	49.5	313	200	4.1	7.54	.08
54	7	Chile	23	56	69.6	138	84	5.5	6.27	.09
55	8	N. Chile	11	32	72.8	143	35	5.4	6.02	.10
56	9	S. Panama	14	11	38.5	129	56	5.1	8.46	.15
57	9	Peru-Ecuador	19	58	49.3	132	108	4.8	7.72	.09
58	11	S. Alaska	17	37	36.6	330	58	5.5	8.49	.09
59	13	S. Bolivia	02	23	72.9	132	589	5.1	6.07	.11
60	May 13	Kamchatka	02	56	62.9	318	100	5.0	6.58	.10
61	13	Columbia	04	13	44.3	124	126	5.3	7.96	.11
62	13	Kurile	16	37	71.0	313	68	4.9	6.08	.10
63	13	Japan	19	23	87.6	308	324	4.8	4.78	.10
64	14	New Hebrides	02	27	92.8	249	259	4.6	4.56	.12
65	14	Fiji	23	28	85.2	240	467	5.3	4.91	.09
66	15	Tonga	23	33	79.3	241	253	4.8	5.51	.10
67	16	Japan	05	40	81.6	311	76	4.3	5.28	.14

TABLE I—*Continued*

No.	Date 1965	Location	Time h	Time m	Δ deg	Azimuth deg	h km	Magni-tude	p sec/deg	RMS Error sec
68	16	Kurile	11	34	71.0	313	11	4.9	6.18	.10
69	16	Panama	15	51	39.4	131	33	4.8	8.41	.13
70	17	Tonga	18	05	82.2	238	75	4.9	5.32	.07
71	17	Komandorsky	20	21	59.0	318	68	5.1	6.88	.15
72	18	Volcano	08	04	88.1	300	10	4.8	4.78	.09
73	18	New Hebrides	08	52	92.6	250	143	5.0	4.56	.14
74	18	New Hebrides	21	29	93.2	251	29	5.0	4.56	.11
75	19	Solomon	03	00	94.9	262	50	5.6	4.67	.05
76	19	S. Fiji	04	21	83.8	237	81	5.5	5.06	.10
77	19	S. Fiji	04	38	83.9	238	98	5.0	5.06	.08
78	19	Columbia	17	58	44.1	124	98	4.8	7.96	.10
79	19	New Britain	13	59	98.1	270	70	5.6	4.53	.19
80	19	Rat	22	07	54.2	313	35	5.3	7.29	.11
81	19	Fiji	23	32	86.3	240	552	5.4	4.86	.10
82	20	New Hebrides	00	40	91.1	253	16	5.6	4.56	.13
83	20	Near	02	13	55.3	312	41	5.4	7.18	.12
84	22	Andreanof	10	24	50.5	312	89	4.6	7.49	.11
85	22	Fiji	10	31	86.7	240	578	5.8	4.81	.08
86	24	Japan	13	48	81.3	310	29	5.0	5.28	.13
87	25	Rat	13	07	52.2	312	40	5.5	7.38	.03
88	27	Argentina	12	18	73.1	137	190	4.5	6.02	.13
89	27	Unimak	12	56	42.0	315	33	5.0	8.09	.15
90	27	Alaska	19	29	37.2	316	33	5.0	8.49	.11
91	May 28	Tonga	08	34	76.8	241	31	5.1	5.76	.10
92	28	Near	18	14	54.8	313	67	5.0	7.29	.12
93	30	Galapagos	19	28	34.6	156	33	4.5	8.57	.17
94	31	Japan	08	38	84.3	309	124	5.5	4.98	.09
95	31	Tonga	09	36	82.8	239	259	4.4	5.26	.10
96	31	Japan	11	23	85.1	305	40	4.8	4.98	.12
97	31	Nicaragua	20	46	32.6	129	28	4.7	8.81	.11
98	June 1	N. Columbia	15	10	45.3	119	152	4.2	7.91	.10
99	2	Chile	02	05	80.6	151	18	5.1	5.43	.08
100	2	Samoa	03	18	76.2	241	33	4.9	5.76	.08
101	2	S. Fiji	05	12	88.9	239	538	5.6	4.66	.09
102	2	Fiji	09	19	85.7	243	631	5.4	4.91	.08
103	2	Easter	13	57	39.0	171	33	5.0	8.42	.14
104	2	Easter	14	06	38.7	171	33	4.7	8.42	.14
105	2	Fiji	14	45	85.7	243	636	5.3	4.91	.09
106	2	Fiji	14	58	85.7	243	636	5.4	4.91	.12
107	2	N. Atlantic	23	40	60.4	90	33	5.8	7.00	.17
108	3	Rat	07	43	53.9	313	49	5.5	7.29	.13
109	3	Dom. Republic	10	57	39.6	103	27	5.3	8.40	.20
110	3	N. Atlantic	12	28	60.1	90	33	4.9	7.00	.14
111	4	Chile	08	05	84.6	155	33	5.4	5.03	.10
112	4	Mariana	13	31	89.9	292	62	4.9	4.69	.14
113	4	Rat	15	02	52.3	311	35	5.3	7.38	.19
114	4	Kermadec	15	26	90.9	234	222	5.3	4.62	.12
115	5	Tonga	11	13	79.3	242	295	5.0	5.51	.08
116	6	Argentina	06	10	72.2	137	122	4.7	6.07	.10
117	11	Easter	01	34	68.8	176	31	5.1	6.28	.05
118	11	Near	02	37	54.8	313	35	5.5	7.29	.14
119	11	Tonga	03	20	78.8	240	95	4.5	5.56	.09
120	11	Kurile	03	33	73.1	313	50	6.0	5.93	.06
121	June 12	Kurile	05	40	73.0	312	24	5.8	5.93	.08
122	12	Sea of Japan	06	19	86.5	318	503	4.6	4.83	.10
123	12	Chile-Bolivia	18	50	67.9	137	102	5.8	6.42	.12
124	13	Kurile	02	20	72.9	312	20	5.5	5.93	.08
125	13	Japan	07	06	77.9	313	34	6.0	5.58	.09
126	13	Kermadec	18	47	91.3	231	33	5.0	4.63	.13
127	14	Mid-Atlantic	16	47	71.6	92	33	5.2	6.15	.16
128	15	Rat	04	46	52.6	310	29	5.5	7.34	.07
129	15	New Zealand	09	20	97.7	229	61	6.2	4.53	.10
130	16	Easter	03	55	68.3	181	33	5.7	6.33	.11
131	16	Japan	04	57	86.3	303	33	5.1	4.83	.08
132	17	E. Kazakh	03	44	95.6	354	0	5.4	4.45	.07
133	17	Unimak	14	23	40.9	315	33	4.5	8.19	.24
134	18	Peru	22	45	58.0	135	111	5.5	7.06	.11
135	18	Japan	22	58	83.7	308	60	4.9	5.08	.08

TABLE I—*Continued*

No.	Date 1965	Location	Time h	Time m	Δ deg	Azimuth deg	h km	Magnitude	p sec/deg	RMS Error sec
136	19	Near	06	38	55.9	314	38	5.5	7.14	.13
137	19	N. Atlantic	11	09	55.1	42	33	4.5	7.48	.31
138	19	Kamchatka	12	50	62.3	318	61	5.1	6.68	.08
139	20	Samoa	00	50	79.0	243	297	4.9	5.56	.10
140	20	Kurile	01	57	72.9	313	41	5.5	5.93	.09
141	20	Kamchatka	21	51	63.8	317	45	4.7	6.53	.06
142	21	N. Columbia	09	27	45.5	119	169	4.1	7.91	.10
143	22	N. Chile	14	19	66.3	136	122	5.0	6.52	.12
144	23	Nicaragua	07	37	31.2	131	24	4.5	8.91	.23
145	23	Kermadec	10	59	91.8	231	23	5.3	4.53	.14
146	23	Kodiak	11	09	35.9	321	33	5.7	8.54	.19
147	23	Kodiak	12	23	35.8	321	33	4.7	8.54	.19
148	24	N. Chile	03	29	65.7	136	72	5.0	6.52	.18
149	24	Japan	04	48	88.0	311	356	5.3	4.73	.10
150	24	Fiji	14	08	84.9	237	102	5.5	5.01	.12
151	June 25	S. Pacific	20	27	72.4	167	33	5.3	6.03	.11
152	26	Chile-Argen.	03	35	74.5	143	119	4.6	5.92	.06
153	26	Andreanof	22	14	50.5	311	43	5.2	7.49	.06
154	26	Cen. Alaska	23	13	37.3	332	75	4.8	8.49	.08
155	27	S. E. Alaska	11	08	32.2	333	12	5.3	8.84	.08
156	27	Peru-Ecuador	17	09	49.3	132	117	5.1	7.72	.08
157	27	Peru-Ecuador	17	09	48.9	132	33	5.3	7.72	.09
158	28	New Ireland	03	33	97.5	269	48	5.5	4.50	.05
159	29	Kurile	02	04	72.8	313	37	5.5	5.93	.08
160	29	Kurile	16	01	71.5	313	48	4.7	6.03	.10
161	29	N. Columbia	20	00	45.6	119	171	4.8	7.96	.32
162	30	Rat	08	33	53.4	313	41	5.7	7.34	.10
163	30	S. Bolivia	11	12	70.6	135	170	5.1	6.22	.08
164	30	Kamchatka	12	36	62.4	318	63	5.1	6.63	.05
165	July 1	Chile	04	54	70.9	138	85	5.1	6.17	.09
166	1	Mariana	07	16	89.8	292	80	5.1	4.69	.12
167	1	Kurile	17	41	64.6	315	50	5.1	6.53	.07
168	2	Rat	20	19	54.0	313	37	5.4	7.34	.14
169	2	Fox	20	58	43.8	313	60	6.7	7.99	.14
170	3	N. Atlantic	02	22	57.3	45	33	5.3	7.38	.29
171	3	Japan	15	24	84.4	309	112	4.5	5.03	.07
172	4	Fiji	09	01	81.0	243	375	4.4	5.41	.11
173	5	N. Atlantic	08	31	56.1	45	30	5.6	7.38	.30
174	5	Chile-Argen.	20	28	77.8	146	90	4.4	5.67	.12
175	6	Loyalty	03	04	91.6	244	54	5.9	4.62	.06
176	6	Greece	03	18	95.8	35	20	5.9	4.58	.15
177	6	Kurile	04	08	69.8	313	39	5.6	6.18	.04
178	6	Kamchatka	04	58	61.0	319	34	5.2	6.74	.07
179	6	Solomon	18	36	97.3	269	510	6.4	4.50	.11
180	July 7	Rat	17	15	54.3	312	28	4.8	7.29	.15
181	7	Samoa	23	02	75.7	242	32	5.1	5.81	.05
182	9	N. Atlantic	16	38	55.2	454	33	4.6	7.44	.28
183	11	Tonga	05	21	77.1	242	52	4.9	5.71	.06
184	11	Kodiak	07	12	35.6	324	7	5.1	8.54	.16
185	11	Iceland	09	52	58.3	33	33	4.7	7.23	.08
186	11	Tonga	20	12	81.9	240	257	4.7	5.36	.08
187	12	Samoa	05	34	77.4	240	62	5.0	5.66	.04
188	12	Unimak	06	43	41.7	315	33	4.3	8.09	.19
189	12	Argentina	13	57	24.8	141	118	5.7	5.87	.07
190	13	Tonga	06	23	80.8	238	63	5.1	5.51	.07
191	13	Andreanof	14	09	50.4	312	55	5.2	7.54	.10
192	14	Alaska	02	29	33.1	324	33	4.5	8.79	.11
193	14	Peru	12	29	65.7	135	146	5.0	6.57	.15
194	14	Galapagos	17	06	38.0	145	33	4.7	8.51	.27
195	15	Santa Cruz	08	01	91.0	255	120	4.8	4.61	.19
196	18	Alaska	07	23	41.2	313	35	4.9	8.14	.19
197	19	Costa Rica	22	14	33.8	129	80	4.6	8.71	.10
198	19	Fiji	23	53	90.0	237	497	4.8	4.67	.10
199	20	Kurile	11	19	67.0	314	49	5.2	6.43	.06
200	20	Fox	20	11	43.2	315	73	5.1	7.98	.14
201	23	Chile-Argen.	11	32	79.1	147	108	4.4	5.58	.08
202	25	Japan	13	33	76.1	311	33	5.8	5.73	.04
203	26	Mid-Atlantic	18	23	70.8	93	33	4.6	6.25	.14

TABLE I—*Continued*

No.	Date 1965	Location	Time		Δ deg	Azimuth deg	h km	Magni- tude	p sec/ deg	RMS Error sec
			h	m						
204	27	Rat	11	20	52.8	312	31	5.4	7.34	.14
205	28	Japan	05	58	84.5	310	149	4.5	4.98	.10
206	29	Fox	08	29	45.9	310	22	6.3	7.89	.09
207	29	Fox	09	32	46.1	310	33	4.5	7.84	.09
208	29	Aleutian	12	20	46.1	310	33	5.5	7.84	.05
209	July 30	Argentina	02	11	75.1	134	524	4.5	5.87	.10
210	30	Chile	05	45	65.0	137	72	6.0	6.57	.14
211	30	N. Columbia	07	20	45.6	119	170	5.5	7.91	.12
212	Aug. 3	N. Peru	02	01	50.2	140	33	5.8	7.52	.05

near 0.5 sec were used. A model of the crust underlying the array was constructed from seismic refraction and gravity data. A computer was used to digitize the array data and to determine the time shifts required to align the P-wave signal on all of the array channels. These relative arrival times were then corrected for the effects of the crust and a value of $p = dT/d\Delta$ determined. (Throughout this paper we will use the symbol p interchangeably with $dT/d\Delta$.) In Figure 1 we have reproduced the seismograms from one of the earthquakes of this study (event number 2 in Table 1). The time shifts which were necessary to obtain the alignment of the P wave as it is shown in this figure were then used to compute a value of p for this earthquake. Note that the seismograms have not been normalized so the amplitude variations are partly due to different gain settings on the various channels.

The P waves from a total of 212 earthquakes in the distance range of 30 to 100° from the center of the array were analyzed. The pertinent information about the earthquakes and the results of the analysis are tabulated in Table 1. The epicenters of the earthquakes are plotted on the map of Figure 2. The location of the array in the southwestern U. S. is also shown. The refined hypocenter locations of the U. S. Coast and Geodetic Survey were used and the Jeffreys velocity structure was used to correct all of the hypocenters to a common source depth of 33 km. For each earthquake a value of p was determined to the nearest 0.05 sec/deg by comparing the observed relative arrival times with tables calculated for various values of p. The root-mean-square residuals between the observed and calculated relative arrival times is also shown in Table 1. A correction for the effect of the earth's ellipticity, which was always less than ±0.03 sec/deg, has already been applied to the p values in Table 1. The p values for earthquakes beyond a distance of 90° from the array also include a correction for the effect of the earth's core which will be explained in a later section.

The measured values of p are plotted in Figure 3. The data were grouped according to the azimuth from which the waves approached the array, and in Figure 3 a different symbol has been used for the different quadrants. In general the scatter in the p data is not more than what one would expect from the accuracy of the measurements. The precision in the p values is estimated to be between 0.025 and 0.050 sec/deg, and, as we will explain later, the standard deviation of a single observation is estimated to be about 0.039 sec/deg.

From Figure 3 it is clear that the majority of the data can be used to define a mean curve of p versus Δ and that the scatter about this curve is fairly small. However, it is also clear that there are a few points which lie a considerable distance from this mean curve and in that sense they are anomalous. Almost all of these anomalous p values can be associated with either of two cases. The first case consists of earthquakes with epicenters on the mid-Atlantic ridge. These particular earthquakes yield p values

which are considerably above the mean curve at the same distances. The second case consists of the earthquakes with epicentral distances greater than 94°. The p values measured in this distance range show a scatter which is much too large to be explained by experimental errors. Therefore, before discussing the rest of the data, we will first consider these two special cases of anomalous data.

THE MID-ATLANTIC RIDGE

Between the distances of 55 and 63° in Figure 3 there are seven data points which lie well above the mean curve described by the rest of the data. All seven of these earth-
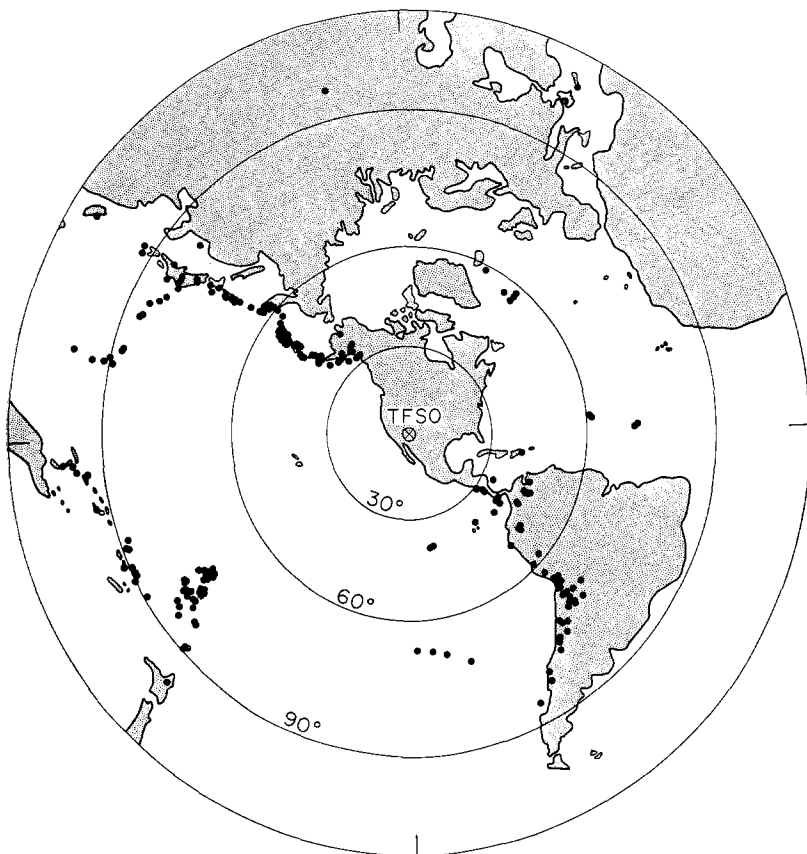
FIG. 2. Epicenters of the earthquakes which were used in this study.

quakes have epicenters near the axis of the mid-Atlantic ridge. The deviations of these data points from the mean curve averages about 0.25 sec/deg which is more than five times the computed standard deviation for a single observation (0.039 sec/deg). Two other earthquakes with epicenters near the axis of the mid-Atlantic ridge were also analyzed and these were at epicentral distances of about 71°. Both of these earthquakes also had measured p values which fell above the mean curve, although the deviations were not as large as for the seven events at the smaller distance range. The deviations for these two events averaged about 0.10 sec/deg which is in excess of two standard deviations of a single observation. Thus we have observations from a total of nine earthquakes from the mid-Atlantic ridge and all of them yield anomalously large p

values. These nine earthquakes correspond to the events numbered 107, 110, 127, 137, 170, 173, 182, 185, and 203 in Table 1 and are easily located on the map of Figure 2.

Having noted that these p values from the mid-Atlantic ridge are anomalous, the next step is to consider some possible explanations. It is reasonable to assume that the anomalous p values result from anomalous velocities along the ray path from the source to the array. The anomalous velocities may be located near the array, in the deep mantle, or near the axis of the mid-Atlantic ridge, and in the following we will consider each of these possibilities in turn.

Consider the possibility that the anomalous velocities are located near the array
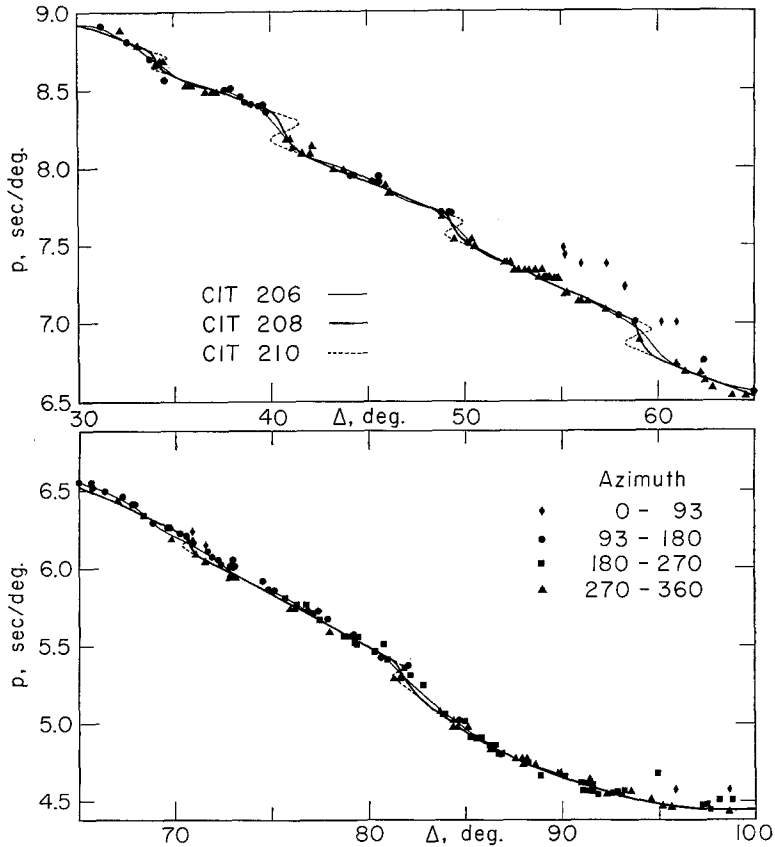
FIG. 3. Measured values of $p = dT/d\Delta$.

One of the results of our study of data from TFSO is that, after corrections are made for the estimated crustal structure beneath the array, the resulting p values show a very small dependence upon the azimuth from which the ray approaches the array. This has led us to the tentative conclusions that the estimated crustal structure is an adequate model and that lateral variations in the velocities of the lower mantle are not great enough to noticeably affect the measured p values. However, these conclusions apply only to those azimuths where we have an adequate number of data, essentially the second, third, and fourth quadrants. We have very few data from the east or north-east (see Figure 2) and most of these are the anomalous events from the mid-Atlantic ridge which we are now considering. The nine events from the mid-Atlantic ridge have azimuths lying in the range of 33° to 93°. Only two other events have azimuths in this range, one from Greece and the other from Crete. Both of these

events also yield what appear to be anomalously large p values. But both of these events are at epicentral distances greater than 96°, and, as we shall see in the next section, their anomalous p values may possibly be related to the diffraction effects of the core. A previous study (Johnson, 1967b) contained only one event with an azimuth similar to the mid-Atlantic ridge (an explosion off the east coast of the U. S. at a distance of 29.8° from TFSO) and this event did not have an anomalous p value. It appears that there are insufficient data to decide whether the anomalous p values from the mid-Atlantic ridge events are actually caused by anomalous velocities near the array. We must retain the possibility that rays approaching the array from the east and northeast are severely distorted by anomalous velocity structures for which we have not corrected. The location of the array near the physiographic boundary between the Basin and Range and the Colorado Plateau makes such a possibility plausible. It may be that the events to the east and northeast are associated with rays that have arrived at the array by passing through an upper mantle which is characteristic of the Colorado Plateau while most other events of this study are associated with rays that have passed through an upper mantle characteristic of the Basin and Range. If such a phenomenon were to explain the data, then the upper mantle velocities of the Colorado Plateau would have to be greater than those at similar depths beneath the Basin and Range.

Next consider the possibility that the anomalous p values from the mid-Atlantic ridge events are caused by anomalous velocities in the lower mantle. At first glance it seems rather improbable that such anomalous velocities should exist within one azimuthal range but that similar anomalies should not be evident in any other azimuthal range. However, inspection of Figure 2 reveals that the ray paths from the mid-Atlantic ridge lie beneath the North American continent and the Atlantic Ocean, while the ray paths of almost all other events in this study lie almost completely beneath the Pacific Ocean or its immediate surroundings. Thus it is possible to explain the anomalous p values from the mid-Atlantic ridge events by postulating a basic difference between the lower mantle underlying the Pacific Ocean and that underlying the North American continent or the Atlantic Ocean.

Finally, consider the possibility that anomalous velocities near the crest of the mid-Atlantic ridge are the cause of the anomalous p values. The existence of anomalously low velocities beneath the axis of the mid-Atlantic ridge appears to be fairly well established. However, decreasing the velocity in the source region tends to decrease the value of p which will be observed at a given distance, and this effect is just the opposite of that which is observed in the p values from the mid-Atlantic ridge. Thus if the low velocities near the crest of the ridge are to explain the observed anomalies, then the region of low velocities must have a geometrical shape such that lateral diffraction will occur. Tryggvason (1961, 1964) has proposed that the northern part of the mid-Atlantic ridge may be underlain by a block of low velocity material (7.4 km/sec) extending down to a depth of 240 km. Rough calculations have shown that such a model is capable of causing lateral diffraction which would explain the observed p values. Thus we have concluded that the anomalous p values could be caused by a block of low velocity material beneath the axis of the mid-Atlantic ridge. Furthermore, from this cursory consideration of three possible causes of the anomalous p values we would surmise that the magnitude of these anomalies could most easily be produced by this third possibility.

From the foregoing discussion it is clear that the earthquakes on the mid-Atlantic ridge have anomalous p values, but the cause of these anomalies is still ambiguous. The

matter is in need of further study with more data. This discussion has also served to point out some of the uncertainties that enter a study such as this when the distribution of the data is incomplete in either the distance range or the azimuthal range.

THE EFFECT OF THE CORE

In the early stages of this investigation as the data began to accumulate and was plotted, it became quite apparent that the scatter in the p values beyond 90° was considerably greater than at lesser distances. Because this apparent scatter could not reasonably be attributed to experimental error, we attempted to find a velocity model which would explain the observed data (Johnson, 1967a). Figure 4a shows the observed data and two fits to the data. The CIT 204 fit is a smooth curve which ignores many of the large values of p beyond 94°. The CIT 204' fit contains a triplication and this added complication allows for a much better fit to the data. This triplication leads to a more complicated velocity model as can be seen in Figure 4b where the lower
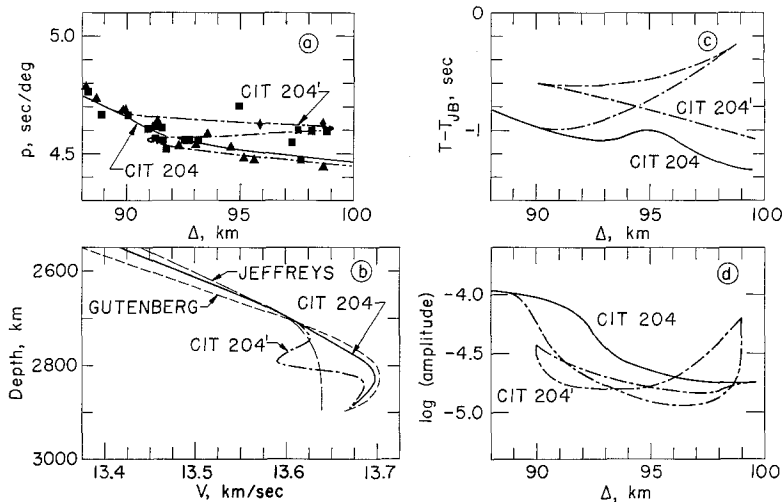
FIG. 4. The measured values of p that relate to the region near the bottom of the mantle and two interpretations of the data.

mantle velocities corresponding to CIT 204 and CIT 204' are plotted along with the models of Gutenberg and Jeffreys. Travel times and amplitudes were also calculated for the two fits to the data and these are shown in Figures 4c and 4d.

Although a model such as CIT 204', which has a fairly complicated structure near the core-mantle boundary, was capable of a much better fit to the observed p values, it was not a completely satisfactory model. First of all, the triplications in travel time predicted by this model were not obvious on the seismograms. Figure 5 shows the seismograms of four events from the distance range beyond 90°. For each event the traces of the 12 array channels were given time shifts appropriate for the listed values of p and are displayed along with their distances from the source. The seismograms in this distance range were definitely more complex than at lesser distances (compare Figure 5 with Figure 1), but it was not possible to establish a pattern of triplication such as that shown in Figure 4c. Another problem with this model was the fact that at certain distances it appears to be rather arbitrary whether the measured value of p lies near the upper or lower branch of the triplication (Figure 4a). Thus our early attempts to analyze the p data beyond 90° can be summarized as follows: The data

definitely indicated some sort of complicated velocity structure near the bottom of the mantle but a satisfactory model had not yet been discovered.

In the initial stages of this investigation it had been assumed that the core had a negligible effect upon the measured p values. However, it was suggested by Robert
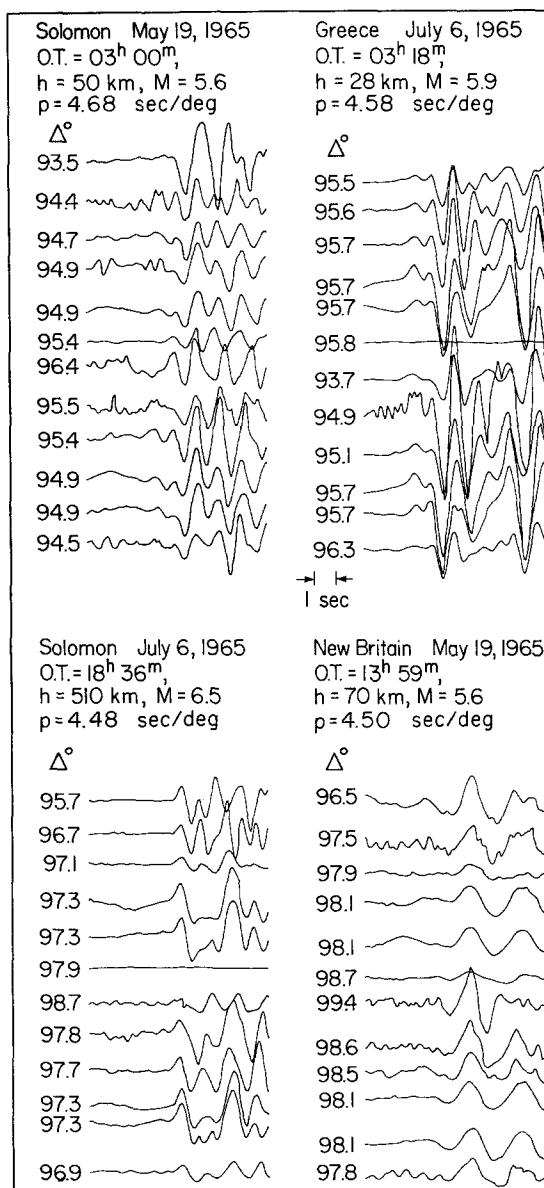
FIG. 5. The seismograms of four events that were observed at distances greater than 90°.

Phinney (personal communication, 1967) that this effect may be appreciable, and so we have taken a more critical look at this problem. Phinney and Alexander (1966) and Phinney and Cathles (1968) have presented a fairly exact theory for calculating the effect of the core upon the seismic waves recorded in either the lit region or the shadow region of the core. In what follows we shall make calculations of this type but we shall use an alternate theory which leads to simpler calculations at the short periods.

The technique which was used to measure the p values amounted to following a given "phase" across the array and measuring its velocity. Thus the measured p values are more directly related to the phase velocity than the group velocity, and we will be interested in calculating the effect of the core upon the phase velocity. This phase velocity will be a function of the period of the phase. For the purpose of making corrections to the measured p values we associated a period with each p value by measuring the time intervals between successive peaks or zero crossings of the initial cycle of the P wave. These estimates of the periods ranged between 0.8 and 2.1 sec.

Let us first consider the P waves in the lit zone fairly close to the shadow boundary. In this zone we can represent the effect of the core as the interference pattern between the P and PcP waves. At a given distance Δ we represent the P waves as

$$g_1(t, \Delta) = A_1(\Delta)f(t) \tag{1}$$

where A_1 is the amplitude of the pulse and f is its shape. Now let the difference in travel time between the P and PcP waves be τ. Then the PcP wave can be represented as

$$g_2(t, \Delta) = A_2(\Delta)R(\Delta)f(t - \tau) \tag{2}$$

where R is the reflection coefficient at the core-mantle boundary. The amplitude factors A_1 and A_2 are a product of two effects, the geometrical spreading of the wave front and the attenuation due to imperfect elasticity. In the limited distance range that we are considering, between about 90° and the shadow boundary, the P and PcP waves have very similar wave paths and it is reasonable to assume that the effects of attenuation upon the two waves will also be very similar. Thus the ratio between A_2 and A_1 will be primarily a function of the geometrical spreading. Letting

$$\alpha(\Delta) = \frac{A_2(\Delta)}{A_1(\Delta)} R(\Delta) \tag{3}$$

we can represent the sum of the two waves as

$$\begin{aligned} g(t, \Delta) &= g_1(t, \Delta) + g_2(t, \Delta) \\ &= A_1(\Delta)[f(t) + \alpha(\Delta)f(t - \tau)]. \end{aligned} \tag{4}$$

The Fourier transform of equation (4) can be written as

$$G(\omega, \Delta) = A_1(\Delta)F(\omega)[1 + \alpha(\Delta)e^{i\omega\tau}] \tag{5}$$

where we have used upper case letters to denote Fourier transforms. So we see that in the frequency domain the effect of the PcP wave is just (also see Pilant and Knopoff, 1964)

$$1 + \alpha(\Delta)e^{i\omega\tau} = [1 + 2\alpha \cos (\omega\tau) + \alpha^2]^{1/2}e^{i\varphi} \tag{6}$$

where

$$\varphi = \tan^{-1}\left(\frac{\alpha \sin(\omega\tau)}{1 + \alpha \cos(\omega\tau)}\right). \tag{7}$$

Finally, the effect of the core upon the p value of the P wave can be written as

$$\delta p = \frac{1}{\omega} \frac{d\varphi}{d\Delta}.$$ (8)

Now φ is a function of α and τ and both of these can be easily calculated as a function of Δ. Thus δp can be calculated as a function of frequency and distance. It should be noted that for transient waves the foregoing analysis can only be used when τ is less than the dominant periods of $f(t)$.

We will now outline the method by which this approximate theory was applied. The measured p values beyond $90°$ were fit with a smooth curve similar to that shown in Figure 7 as a first approximation. The amplitude data of Sacks (1966) has indicated that the shadow boundary of the core lies near $96°$ and we assumed a value of $97°$. The p curve for the P waves was then inverted to obtain a velocity model for the mantle, and this was used to calculate a p curve for the PcP waves. The shape of the p curve for PcP waves is relatively insensitive to changes in the velocity model used in its calculation. With the p curves for both P and PcP now available it was straightforward to calculate the ratio of the geometrical spreading factors for the two waves. Next we adopted a core-mantle boundary like that of the Gutenberg-Bullard I model (Bullard, 1957) and calculated the reflection coefficient for the PcP wave by assuming a plane boundary. Thus the quantity α (equation 3) could be determined as a function of Δ. The quantity τ was determined by integrating the area between the p curves of the P and PcP waves. Then φ was calculated as a function of distance and frequency (equation 7) and the first differences of the result were used to determine δp (equation 8).

Now let us consider the P waves within the shadow of the core. Following Scholte (1956, p. 29) we can represent a harmonic wave in this region by

$$g(t, \Delta) = A \ (\sin \Delta)^{-1/2} \exp \left[-i\omega t\right] \sum_{n=1}^{\infty} \nu_n^{-1/2} \exp \left[i\nu_n \Delta_s (\omega p)^{1/3}\right]$$ (9)

where A is a constant, Δ_s is the distance from the shadow boundary, and ν_n is the nth complex root of an equation given by Scholte (1956, p. 31). At large frequencies we can safely assume a hollow accoustic sphere (see Phinney and Alexander, 1966, Figure 3) and then the roots are given by

$$\nu_n = \frac{1}{2} \ (4n - 1)^{2/3} \left(\frac{3\pi}{4}\right)^{2/3} \exp \left[\frac{i\pi}{3}\right].$$ (10)

An n increases the imaginary part of ν_n increases and the relative contribution of the corresponding term to the sum of equation 9 decreases rapidly. It is customary to consider only large values of Δ_s and then only the first term of the sum need be included. Because we were interested in obtaining results for fairly small values of Δ_s we included all terms through $n = 10$. The Fourier transform of equation 10 was calculated, the results were separated into a modulus and phase, and then equation 8 was used to calculate the perturbations in the p values.

In Figure 6 the results of the calculations for both the lit and shadow regions are shown. The curve for zero period represents the unperturbed p curve for P waves. The other three curves represent the p curves which one would expect to observe for

the corresponding periods. The dashed portions of these curves near the shadow boundary were extrapolated because the methods used in both the lit and shadow regions fail near this boundary. Each measured p value in the distance range beyond 90° was corrected for the effect of the core by determining a value of δp for the appro-
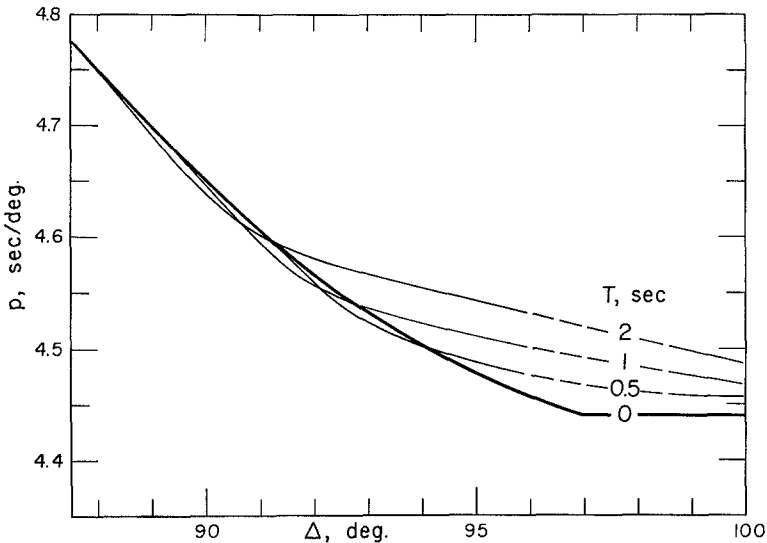
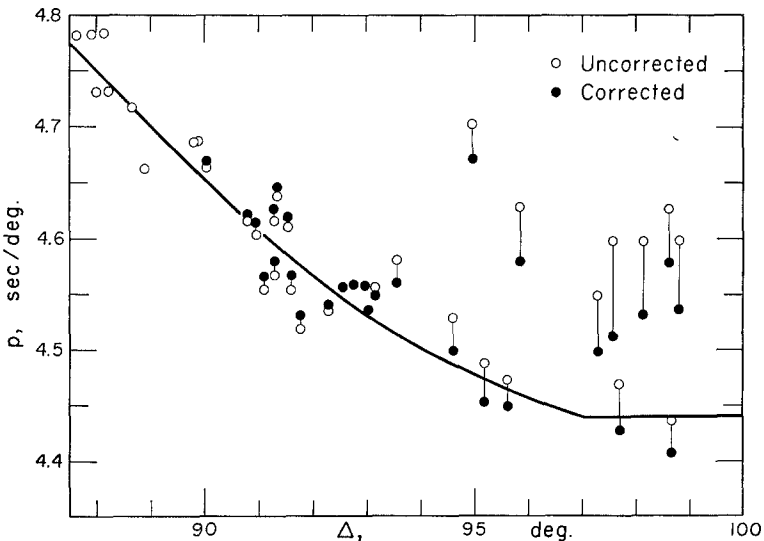FIG. 6. Calculated values of p for four different values of the period T.

FIG. 7. The p values in the distance range beyond 90° both before and after corrections were made for the effect of the core.

priate distance and period and subtracting this from the measured value. Figure 7 shows the p values both before and after the corrections were made. The p values listed in Table 1 and plotted in Figure 3 are the corrected values. The final fit to the data is also shown in Figure 7. It should be pointed out that in drawing this curve we have attempted to make it as smooth as possible and in doing so we have tended to weight the shorter period data more heavily than the longer period data. This seemed reasonable

in view of the facts that the calculated corrections are only approximate and the shorter period data are least affected by the corrections

In Figure 7 it is clear that the corrected p values are much easier to approximate by a smooth curve than the uncorrected values. In practically every case the sense of the correction has been to move the points toward the curve shown in the figure. The scatter in the data still remains considerably greater than at smaller distances but there are several reasons why one might expect this. First of all, the corrections to p are calculated with an approximate theory and an approximate model. Secondly, lateral variations in the structure near the core-mantle boundary such as suggested by Alexander and Phinney (1966) may introduce scatter into the data. Finally, the validity of our technique of measuring p is questionable in the range beyond 90°. A much better technique would be to Fourier analyze the seismograms and then compute p as a function of frequency. Such an analysis coupled with theoretical calculations according to the method described by Phinney and Cathles (1968) might provide fairly detailed information about the structure near the core-mantle boundary.

Note that only three of the corrected p values in Figure 7 (also see Figure 3) show large discrepancies. The one near a distance of 95° is from the Solomon Islands (event 75 in Table 1) and the reason for the discrepancy in its p value remains unexplained. The other two large p values correspond to an earthquake from Greece at a distance of 95.8° (event 176 in Table 1) and one from Crete at a distance of 98.6° (event 29 in Table 1). The discrepancies in these p values are also unexplained, but it is interesting to note that these events are in the same azimuthal range as the earthquakes from the mid-Atlantic ridge which also yielded anomalously large p values.

Two main conclusions have emerged from our consideration of the effect of the core upon measured p values beyond 90°. First, the correction for the effect of the core is of large enough magnitude so that it must be applied to the data. Second, after the correction has been applied, the data no longer contain compelling evidence for a complicated velocity structure near the core-mantle boundary. Some other ramifications of the correction for the effect of the core will become apparent when we describe the inversion of the p data.

ANALYSIS OF THE DATA

Now let us return to the consideration of the majority of the data shown in Figure 3. If we omit the data from the mid-Atlantic ridge and also the data beyond 90° we are left with 174 measured p values between 30 and 90°. We wish to fit these data with a curve and then use the Wiechert-Herglotz method to obtain the compressional velocity as a function of depth in the earth. In order to discuss the relative merits of various fits to the data we shall need an estimate of the standard deviation of a single observation, and so we will first describe the estimation of this quantity.

The precision of the measured p values is estimated to be between 0.025 and 0.050 sec/deg. However, there are other sources of scatter due to the fact that at any given distance we are grouping together data from different sources and different azimuths. Thus the precision of the measurements is not a good estimate of the standard deviation. Our method of estimating the standard deviation was as follows: The data between 30 and 90° were fit with a least-squares straight line. The residuals from this line were then calculated and grouped into 2° cells with an average of 5 to 6 residuals in each cell. This method succeeds in removing practically all of the distance dependence from the data. The mean and variance of each cell were calculated and the variances of all the cells were summed. This method yielded a standard deviation of 0.039 sec/deg

on 144 degrees of freedom. We have used this number as the computed standard deviation for a single observation of p.

We first attempted to fit the p data between 30 and 90° with a straight line. Least-squares analysis yielded

$$p = (11.176 \pm 0.020) - (7.188 \pm 0.030) \times 10^{-2}\Delta. \qquad (11)$$

This fit gave a χ^2 of 554 on 172 degrees of freedom which is not a satisfactory fit to the data. (In this paper we shall follow the convention that for ν degrees of freedom a computed χ^2 in the interval $\nu \pm \sqrt{2\nu}$ is consistent with a true hypothesis and random errors.) Next we tried to fit the data with a quadratic and this yielded

$$p = (10.659 \pm 0.164) - (5.352 \pm 0.227) \times 10^{-2}\Delta$$

$$- (1.494 \pm 0.183) \times 10^{-4}\Delta^2. \qquad (12)$$

This fit gave a χ^2 of 426 on 171 degrees of freedom which is still not a satisfactory fit. From these results we concluded that there might be some difficulty in fitting the data with a simple polynomial.

One method of fitting the data which was guaranteed to satisfy the χ^2 test was to use essentially the same method we had used to estimate the standard deviation. The residuals from the straight-line fit were calculated and grouped into 2° cells. The means of the residuals in the various cells were then connected with a smooth curve, and the result has been labeled CIT 206 in Figure 3. Although this is a satisfactory fit to the data, 30 parameters are required to specify the curve and this is a rather large number. Thus we continued to search for a satisfactory fit with a fewer number of parameters.

The p data in Figure 3 give the distinct impression of defining a number of straight line segments which are offset from each other. Over distances of several degrees the data can be fit quite well by an essentially straight line, and it is possible to fit the entire distance range with seven lines of this type. These line segments are not continuous and are offset from each other at the distances where they begin to overlap. The curve labeled CIT 208 in Figure 3 is such a fit to the data. It consists of seven very smooth segments joined by six small offsetting segments, and thus it can be specified by about 14 parameters. This fit gives a χ^2 of 169 on 160 degrees of freedom which is acceptable. Application of the F distribution shows that the difference between the variances of the CIT 206 and CIT 208 curves is not significant at the 5 per cent level. Thus the CIT 208 curve is also a satisfactory fit to the data and has an advantage over the CIT 206 curve in that it can be specified by a considerably smaller number of parameters.

Fitting the p data with a curve such as the CIT 208 curve results in some interesting implications about the velocity structure of the lower mantle. Each of the abrupt offsets of the p curve indicates a region of the mantle where the velocity gradient is anomalously large. These offsets in the p curve are very similar to those which have been found in the studies of the upper mantle (Niazi and Anderson, 1965; Johnson, 1967b; Kanamori, 1967), except that the magnitude of the offsets are at least an order of magnitude smaller in the lower mantle. In a previous study of the upper mantle (Johnson, 1967b) it was possible to show that the offsets in the p curve were actually triplications and this allowed us to approximate the actual shape of the high-gradient

regions in the upper mantle. In the present case of the lower mantle we have been unable to do this and the manner in which the offsetting segments of the CIT 208 curve have been drawn is rather arbitrary. It is conceivable that triplications also exist in the lower mantle p curve, and so the curve labeled CIT 210 in Figure 3 is another possible fit to the data. Except for the regions of the triplications this curve is identical to the CIT 208 curve. A study of the seismograms to determine if these triplications were present was indecisive. It can be shown that the differences between the travel times of the various branches of the triplications are never more than 0.2 sec so one would expect some difficulty in observing them.

The CIT 208 and CIT 210 curves in Figure 3 have offsets near distances of 34.5, 40.5, 49.5, 59.5, 70.5, and 81.5°. All of these distances are uncertain by about 0.5°. The offset near 70.5° is small and poorly defined, and that near 34.5° is also small. But the offsets near 40.5, 49.5, and 59.5° are all large and fairly well defined. The feature of the p curves near 81.5° is more like a second-order discontinuity than an actual offset. It is important to realize that the scheme used to fit the CIT 208 and CIT 210 curves to the p data has tended to emphasize the anomalously steep portions of the curve. It is obvious that one could use other schemes which would place more emphasis on portions of the p curve that are anomalously flat. On the other hand the CIT 206 curve was fit to the p data by a scheme that contained no predisposition about the shape of the curve. Although this curve contains both regions that are flatter than average and those that are steeper than average, the steep regions appear to be the more outstanding. The CIT 206 curve contains anomalous features similar to the CIT 208 curve near the distances of 40.5, 49.5, 59.5, and 81.5°.

We have tentatively concluded that the p data actually contain some of the anomalous features which are exhibited by the curves in Figure 3. However, this fact by itself is not sufficient to prove the existence of corresponding features in the velocity structure of the lower mantle. Although our analysis of the data from the mid-Atlantic ridge was only qualitative, it was clear that velocity anomalies in the source region may cause appreciable anomalies in the observed p values. Thus, if we consider data from only one azimuth, the possibility is always present that some anomalous feature in the p data results from the fact that the corresponding distance is the boundary between two source regions with different upper mantles. To a limited extent, all of the offsets in the CIT 208 and CIT 210 curves are based upon data from more than one azimuth and this greatly increases the probability that they are caused by velocity structures in the lower mantle. In a later section we will consider some other types of data that relate to this same problem.

The p data in Figure 3 are plotted with different symbols to denote the azimuth from which the wave approached the array. Besides the data from the mid-Atlantic ridge which we have already discussed, there is no obvious azimuthal dependence in the data. But this matter can be easily handled in a more quantitative manner. We assumed the CIT 208 curve to be a reasonable good approximation to the distance dependence in the data and calculated the mean residuals of the data from this curve for various azimuths. From Figure 2 it is clear that the four quadrants provide a convenient grouping of the data. Again we confined this analysis to the data between distances of 30 and 90°. All 9 data in the first quadrant are from the mid-Atlantic ridge and have a mean residual of 0.198 sec/deg. The second quadrant is represented by 57 events from Central America, South America, and the southeast Pacific and these events have a mean residual of 0.019 sec/deg. The third quadrant contains 30 events from the islands of the southwest Pacific such as Fiji, Tonga, Samoa, etc., and their mean residual is

0.005 sec/deg. The fourth quadrant contains 87 events from Alaska, the Aleutian arc, the Kurile-Kamchatka arc, Japan, and the Mariana Islands. Its mean residual is −0.014 sec/deg.

These residuals confirm our original estimate that the azimuthal effect is much larger in the first quadrant than in any of the other quadrants. Application of Student's t distribution indicates that the following conclusions are valid at the 5 per cent level of significance: (a) The mean residual of the first quadrant is larger than the mean residuals of all the other quadrants. (b) The mean residuals in the second and third quadrants are both larger than the mean residual of the fourth quadrant. (c) The mean residuals in the second and third quadrants are not different from each other. These results indicate that even after the events from the mid-Atlantic ridge are excluded there may be a small but real azimuthal dependence in the data. As is the case of the data from the mid-Atlantic ridge, we cannot say whether this dependence is due to effects near the array, in the deep mantle, or near the sources.

We also considered the effect of focal depth upon the p data. As mentioned earlier, the focal depths were obtained from the refined hypocenter locations of the U. S. Coast and Geodetc Survey and were corrected to a common depth of 33 km by means of Jeffreys velocity model. We grouped the data in the distance range between 30 and 90° according to whether the focal depth was less than 60 km, between 60 and 300 km, or greater than 300 km. We again used the residuals of the p values from the CIT 208 curve and calculated the mean residual for each of the three ranges of focal depths. For focal depths less than 60 km 96 events gave a mean residual of −0.008 sec/deg. In the range between 60 and 300 km we had 63 events with a mean residual of 0.013 sec/deg. There were 15 events with focal depths greater than 300 km and they had a mean residual of −0.002 sec/deg. We again applied Student's t distribution and found that at the 5 per cent level the mean residual for events with focal depths less than 60 km is significantly different from the mean residual for the events in the 60 to 300 km range, but this was the only significant difference between the three ranges of focal depths.

From the results listed in the above paragraph it appears that the p data may contain a small dependence upon focal depth. However, this apparent dependence upon focal depth may be interrelated with the apparent dependence upon azimuth. The focal depth range between 60 and 300 km which has the largest mean residual consists mainly of events with azimuths in the second quadrant, and this quadrant has a larger mean residual than either the third or fourth quadrants. Thus it is not possible for us to say whether these positive residuals are actually due to the effect of focal depth or the effect of azimuth. However, we have tentatively concluded that, regardless of whether the apparent effects of azimuth and focal depth are real or not, the magnitude of these effects is not large enough to seriously interfere with the process of fitting a mean curve to the data.

VELOCITY MODELS

Given a curve of p versus Δ, such as any of those shown in Figure 3, it is straightforward to apply the Wiechert-Herglotz method (Bullen, 1963, p. 119) to obtain velocities as a function of depth in the Earth. The data of this study begins at a distance of 30° which corresponds to a depth of about 740 km, and so the velocities above this depth must be known before the Wiechert-Herglotz method can be applied. Thus the results we obtain for the lower mantle will depend upon a knowledge of the velocities in the upper mantle.

In a previous study (Johnson, 1967b) we derived a model for the P velocities in the

upper mantle beneath TFSO by studying $dT/d\Delta$ data observed at distances less than 30°. The model which resulted was consistent with both the $dT/d\Delta$ data and the anomalous P delay which has been observed at TFSO. This model, which was labeled CIT 204, was considered to be appropriate for the Basin and Range province where the array is located. It has a velocity of only 7.85 km/sec at the top of the mantle and a pronounced low-velocity zone between depths of 60 and 150 km. In order to obtain a velocity model appropriate for the upper mantle of an "average" region, we modified the CIT 204 model by slightly increasing the velocities in the upper 150 km. This "average" modification of the CIT 204 model was consistent with average travel times at teleseismic distances.

These methods and results of the previous study were also used in the derivation of the lower mantle velocities. Both of the velocity models for the upper 160 km of the Earth that are listed in Table 2 were used in the inversion of the p data. The M model was used for the upper mantle velocities below the array. The R model was assumed for

TABLE 2
VELOCITY MODELS FOR THE CRUST AND UPPER MANTLE

Depth km	Model M Velocity km/sec	Model R Velocity km/sec
0	6.200	6.200
33	6.200	6.200
33	7.850	8.000
40	7.860	8.020
50	7.870	8.040
60	7.870	8.050
70	7.640	8.050
80	7.600	7.955
90	7.600	7.950
100	7.605	7.950
110	7.630	7.953
120	7.670	7.960
130	7.734	7.972
140	7.810	7.990
150	7.930	8.026
160	8.150	8.150

the upper mantle velocities below the source. Note that the two models are identical below a depth of 150 km. The Wiechert-Herglotz method was then applied to the three curves in Figure 3 to obtain corresponding velocity models for the mantle. In the present analysis we actually included all of the p data between 10 and 100° and calculated velocity models for the entire mantle. However, the results for the upper mantle were essentially identical to those presented in the previous paper (Johnson, 1967b) so the upper mantle will not be discussed in the present paper. Because of improvements in our technique the M and R models of Table 2 are slightly different from the corresponding models of the previous paper.

We shall propose that the velocity models that result from the inversion of the p data are estimates of the "average" velocities in the lower mantle, and so our use of the term "average" has to be clearly explained. Earlier we showed that when p data from a great number of source regions covering a large range of azimuths were grouped together the azimuthal dependence, the focal depth dependence, and the random scatter in the data were all small enough so that it was meaningful to define an "aver-

age" p curve. Because the source regions were so numerous and so widely scattered, we assumed an "average" upper mantle for the source region. The upper mantle below the array was common to all the data and was thought to be reasonably well known from a previous study, so we made explicit corrections for that part of the ray path. With these two upper mantle models and the "average" p curve we then obtained a velocity model for the lower mantle. Subject to the condition that our assumptions and procedure are correct, this velocity model should represent an unbiased estimate of the "average" velocities in the lower mantle. Note however, that we included only data from the Pacific Ocean basin and its immediate surroundings, and thus the results are only appropriate as an average for this general region.
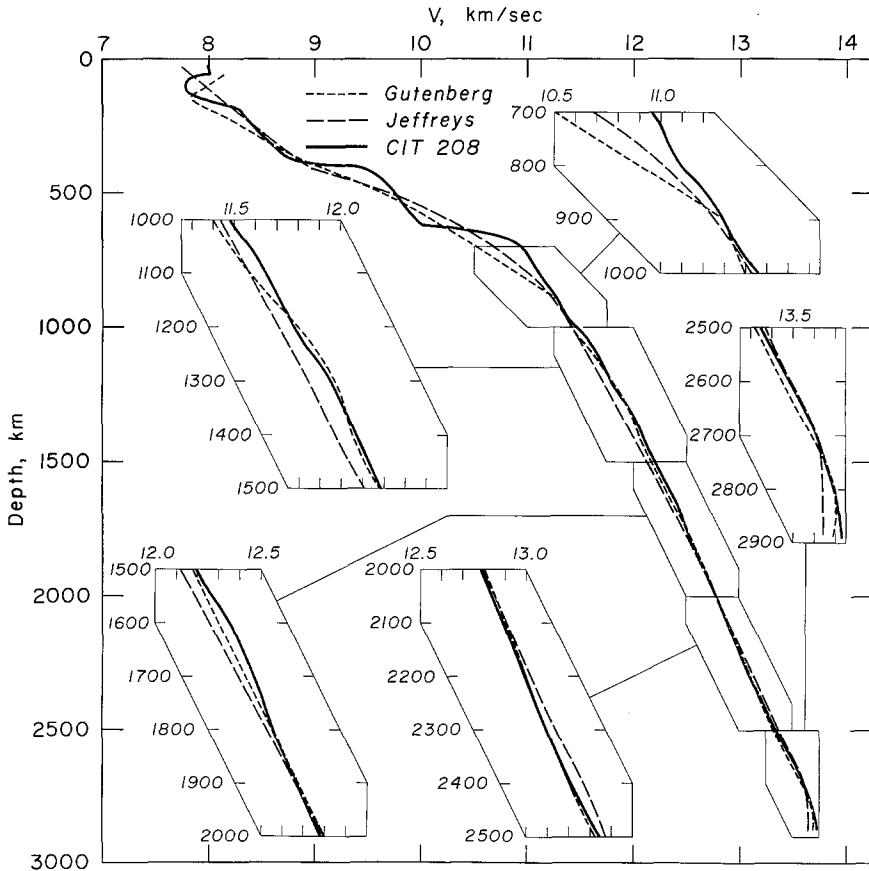
FIG. 8. Velocity models for P waves in the mantle.

The weakest part of the argument presented in the previous paragraph involves the upper mantle model which was assumed for the source regions. This was said to be an "average" upper mantle model because it is in fair agreement with average travel times, such as those of Carder et al. (1966) and Herrin et al. (1968b). But these average travel times were derived for stable continental regions such as the central U. S. (Herrin and Taggart, 1968), and there seems to be no a priori reason why the tectonic source regions of this study should have the same travel times. In fact, it would seem more reasonable to expect anomalous velocity structures in these source regions. In spite of these considerations, there is one very important reason why the "average" upper mantle model is a good choice for the source regions. The earthquakes used in

TABLE 3
COMPRESSIONAL VELOCITIES OF THE CIT 208 MODEL

Depth* km	Velocity km/sec	Depth km	Velicity km/ sec	Depth km	Velicity km/sec	Depth km	Velocity km/sec	Depth km	Velocity km/sec
0	6.200	590	9.920	1170	11.734	1750	12.512	2330	13.118
33	6.200	600	9.948	1180	11.746	1760	12.522	2340	13.130
33	8.000	610	9.982	1190	11.759	1770	12.531	2350	13.142
40	8.020	620	10.044	1200	11.773	1780	12.541	2360	13.154
50	8.040	630	10.241	1210	11.788	1790	12.550	2370	13.168
60	8.050	640	10.412	1220	11.805	1800	12.559	2380	13.181
70	8.050	650	10.560	1230	11.823	1810	12.569	2390	13.195
80	7.955	660	10.679	1240	11.841	1820	12.578	2400	13.209
90	7.950	570	10.782	1250	11.859	1830	12.587	2410	13.224
100	7.950	680	10.856	1260	11.877	1840	12.597	2420	13.238
110	7.953	690	10.905	1270	11.894	1850	12.606	2430	13.252
120	7.960	700	10.944	1280	11.910	1860	12.616	2440	13.266
130	7.972	710	10.968	1290	11.926	1870	12.625	2450	13.280
140	7.990	720	10.985	1300	11.941	1880	12.635	2460	13.294
150	8.026	730	10.998	1310	11.956	1890	12.646	2470	13.308
160	8.150	740	11.011	1320	11.969	1900	12.658	2480	13.322
170	8.287	750	11.025	1330	11.983	1910	12.670	2490	13.336
180	8.304	760	11.039	1340	11.996	1920	12.683	2500	13.350
190	8.311	770	11.054	1350	12.008	1930	12.696	2510	13.364
200	8.321	780	11.069	1360	12.021	1940	12.709	2520	13.377
210	8.336	790	11.084	1370	12.033	1950	12.721	2530	13.391
220	8.355	800	11.100	1380	12.046	1960	12.733	2540	13.404
230	8.376	810	11.119	1390	12.058	1970	12.745	2550	13.418
240	8.398	820	11.138	1400	12.069	1980	12.756	2560	13.431
250	8.421	830	11.160	1410	12.081	1990	12.767	2570	13.444
260	8.445	840	11.183	1420	12.093	2000	12.778	2580	13.458
270	8.469	850	11.206	1430	12.104	2010	12.789	2590	13.471
280	8.493	860	11.225	1440	12.116	2020	12.800	2600	13.484
290	8.518	870	11.243	1450	12.127	2030	12.811	2610	13.496
300	8.542	880	11.259	1460	12.138	2040	12.822	2620	13.509
310	8.567	890	11.275	1470	12.149	2050	12.832	2630	13.521
320	8.592	900	11.290	1480	12.160	2060	12.843	2640	13.534
330	8.618	910	11.304	1490	12.173	2070	12.853	2650	13.545
340	8.647	920	11.318	1500	12.186	2080	12.864	2660	13.557
350	8.678	930	11.332	1510	12.200	2090	12.874	2670	13.569
360	8.713	940	11.346	1520	12.216	2100	12.884	2680	13.580
370	8.759	950	11.361	1530	12.232	2110	12.894	2690	13.591
380	8.831	960	11.378	1540	12.248	2120	12.904	2700	13.601
390	8.953	970	11.397	1550	12.265	2130	12.915	2710	13.612
400	9.311	980	11.417	1560	12.282	2140	12.925	2720	13.622
410	9.421	990	11.438	1570	12.299	2150	12.935	2730	13.631
420	9.501	1000	11.459	1580	12.316	2160	12.945	2740	13.641
430	9.560	1010	11.481	1590	12.332	2170	12.955	2750	13.650
440	9.602	1020	11.503	1600	12.347	2180	12.965	2760	13.659
450	9.632	1030	11.524	1610	12.361	2190	12.975	2770	13.668
460	9.657	1040	11.544	1620	12.374	2200	12.985	2780	13.676
470	9.679	1050	11.562	1630	12.386	2210	12.995	2790	13.684
480	9.700	1060	11.580	1640	12.398	2220	13.005	2800	13.691
490	9.721	1070	11.596	1650	12.409	2230	13.015	2810	13.698
500	9.742	1080	11.612	1660	12.420	2240	13.025	2820	13.704
510	9.762	1090	11.627	1670	12.431	2250	13.035	2830	13.710
520	9.782	1100	11.641	1680	12.442	2260	13.045	2840	13.715
530	9.801	1110	11.656	1690	12.452	2270	13.055	2850	13.719
540	9.820	1120	11.669	1700	12.463	2280	13.065	2860	13.722
550	9.839	1130	11.683	1710	12.473	2290	13.076	2870	13.724
560	9.858	1140	11.696	1720	12.483	2300	13.086	2880	13.725
570	9.878	1150	11.709	1730	12.493	2310	13.096	2890	13.726
580	9.898	1160	11.722	1740	12.502	2320	13.107		

* The radius of the earth is taken as 6371 km.

this study were located by the U. S. Coast and Geodetic Survey without the use of source corrections, and this is equivalent to assuming an averare upper mantle near the source. Thus, if the source region is actually one of anomalous velocities, the solution for the hypocenter will not be the true hypocenter but an apparent hypocenter that would be appropriate for an average upper mantle. For this reason it is appropriate to use an average upper mantle for the source region when the velocity inversion is performed. Also note that the actual velocity structure within the upper mantle model which we assume for the source region is of no consequence so long as the total travel times for rays passing through the model at small angles of incidence are "average." Thus we could have assumed any model that had these "average" travel times without affecting the results for the lower mantle.

The CIT 208 velocity model for P waves is shown in Figure 8 and tabulated in Table 3. The upper mantle velocities of this model are identical to the R model of Table 2.
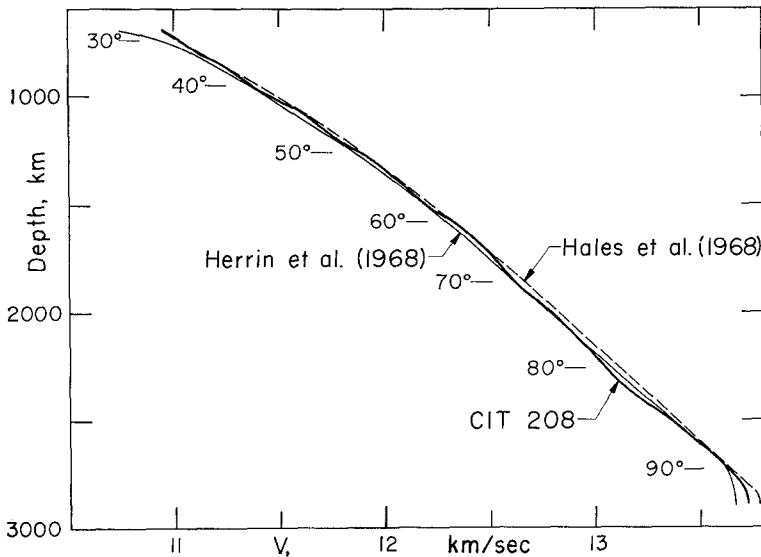
FIG. 9. Three recently determined velocity models for P waves in the lower mantle. The epicentral distances corresponding to different maximum depths of penetration are indicated.

The traditional velocity models of Jeffreys and Gutenberg (Press, 1966) are also shown in Figure 8. There are no large discrepancies among the lower mantles of the three models shown in this figure; below a depth of 900 km the differences among the models are never greater than 0.12 km/sec. In general the CIT 208 model agrees slightly better with Gutenberg's model than with that of Jeffreys.

Although the gross features of the three models shown in Figure 8 are very similar throughout the lower mantle, there are some differences in their fine structure. The Jeffreys model is very smooth throughout the lower mantle. Between 800 and 1000 km it contains a smooth transition from the velocity gradients of the upper mantle to the much smaller velocity gradients of the lower mantle. The Gutenberg model contains a certain amount of fine structure. The transition from the upper mantle velocity gradients to the lower mantle velocity gradients occurs near 900 km. Between 900 and 1000 km the velocity gradient is anomalously small, between 1100 and 1200 km it is slightly larger than average, and around 1400 km it is smaller than average.

The CIT 208 model contains anomalously large velocity gradients near the approxi-

mate depths of 830, 1000, 1230, 1540, and 1910 km. These features correspond to the offsets in the *p* curve near the epicentral distances of 34.5, 40.5, 49.5, 59.5, and 70.5° respectfully. The high-gradient regions are spread over depth intervals of at least 50 km so it is somewhat ambiguous to assign a single depth to them. The depths listed above correspond to the points where the velocity gradient is a maximum. Near a depth of 2370 km there is a fairly abrupt increase in the velocity gradient and this corresponds to the second order discontinuity in the *p* curve near the epicentral distance of 81.5°.

In Figure 9 we have compared the CIT 208 model with two of the most recent velocity models for the lower mantle. These models (Hales *et al*, 1968; Herrin *et al*, 1968a) were both calculated from average travel-time curves. The differences among
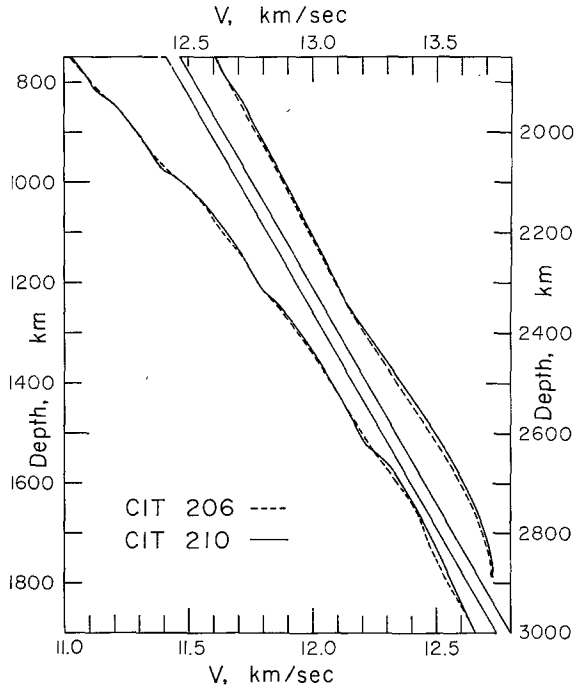
FIG. 10. Velocity models for the lower mantle that have resulted from two different fits to the *p* data of this study.

the three velocity models of this figure are fairly small; below a depth of 800 km these differences are never more than about 0.05 km/sec. Note that throughout most of the lower mantle the CIT 208 model lies between the two parallel models of Hales and Herrin. The main differences among the models lie in their fine structure. The models of Hales and Herrin are both very smooth whereas the CIT 208 model contains the high gradient regions which we have already discussed. Each of the three velocity models of Figure 9 is the result of an independent study and so one can regard their differences as a rough measure of the accuracy with which we know the average velocities of the lower mantle.

The velocity models corresponding to the CIT 206 and CIT 210 curves of Figure 3 were also calculated. The differences among the three velocity models which resulted from different fits to the *p* data are so small that it is difficult to display them in graphical form. Figure 10 is an attempt to compare the velocities of the CIT 206 and

CIT 210 models. The CIT 208 model is almost identical to the CIT 210 model so it was not included in this figure. The maximum difference between the velocities of the three models is 0.02 km/sec. From Figure 10 it is clear that the shapes of the CIT 206 and CIT 210 models are also very similar. The CIT 206 model has high gradient regions near the depths of 830, 1000, 1230, and 1540 km although these regions are smeared out over a greater depth interval than those of the CIT 210 model.

TRAVEL TIMES AND AMPLITUDES

The velocity models of this study have been derived from measured p values, and thus a comparison of their travel times with observed travel times serves as an independent check upon the models. In the past few years there have been several detailed analyses of observed travel times such as those of Kogan (1960), Jeffreys (1962), Carder (1964), Carder et al (1966), Cleary and Hales (1966), Gogna (1967), Hales et al (1968), and Herrin et al (1968b). Most of these studies have yielded similar results and we have reproduced the results of only two of these studies in Figure 11. The trave
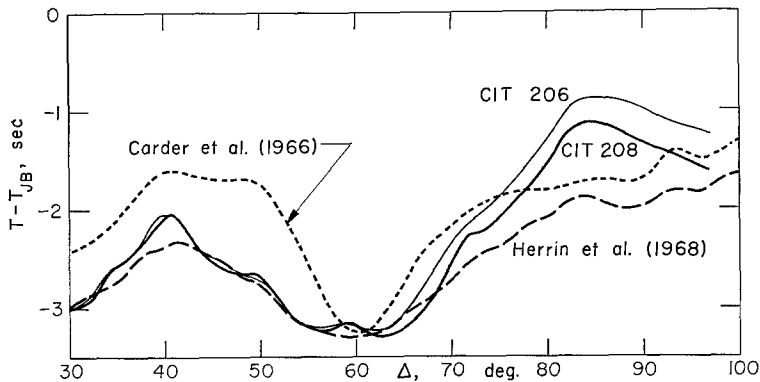
FIG. 11. Travel-time residuals from the Jeffreys-Bullen tables. The residuals of the CIT 206 and CIT 208 models were calculated while those of Carder and Herrin were derived from studies of observed data.

time residuals of Carder et al (1966) are based completely on explosion data. The results of Herrin et al (1968b) are based upon a comprehensive study of both earthquakes and explosions.

The travel times that were calculated for the CIT 206 and CIT 208 models are also shown in Figure 11. The agreement between the observed and calculated travel times is very good both in terms of the shapes of the curves and their absolute values. This figure contains two approximate estimates of the uncertainties involved. The two curves based on the observational data are from independent studies so their difference is an estimate of the uncertainties in the observational data. However, such a comparison is valid only for the shapes of the curves because a constant shift of one curve with respect to the other is allowable. The two curves based on the CIT models were derived from two fits to the same p data so their difference is a lower bound on the uncertainty involved in the present study.

The only appreciable difference between the observed and calculated travel times exists in the range between 73 and 83°. In this range the calculated residuals are increasing at a faster rate than the observed residuals. The fit to the p data is reasonably good in this distance range so this difference remains unexplained. In terms of the

velocity models it corresponds to the depths between about 2000 and 2450 km where the velocities of the CIT models are less than those of most other models (see Figure 9).

Travel times were also calculated for the CIT 210 model but these times were almost identical to those of the CIT 208 model. One can check this result by noticing that the areas beneath the corresponding *p* curves of Figure 3 are almost identical. The travel times of the CIT 210 model has small triplications that correspond to the triplications in the *p* curve. The total separation of the various branches of the triplications is always less than 0.2 sec.

We also measured the absolute travel times to the center of the array for all 212 earthquakes, and in Figure 12 we have plotted these times as residuals from the Jeffreys-Bullen tables. The data have been corrected for ellipticity. The scatter in the times is very great and this illustrates the difficulty of deriving a travel-time residual curve from raw earthquake data such as this. However, it is clear that most of the data
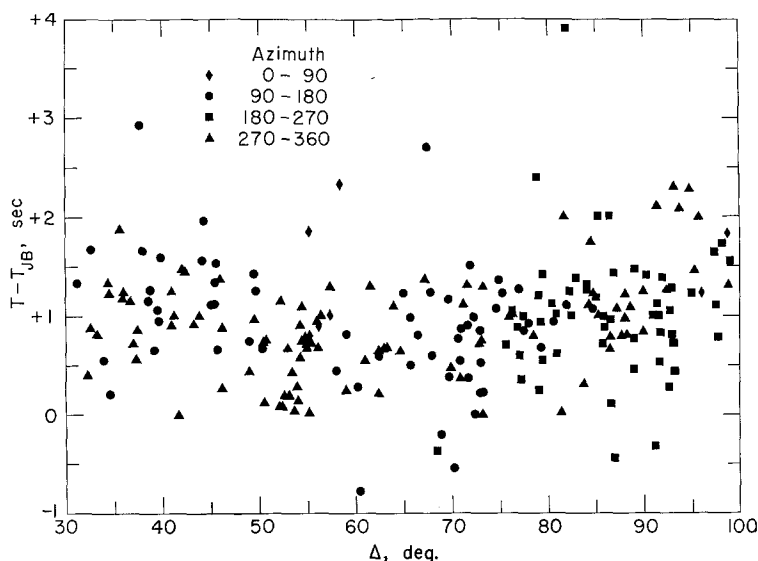
FIG. 12. Travel time residuals from the Jeffreys-Bullen tables that were observed at TFSO for the earthquakes of this study.

are greater than zero which confirms the positive station anomaly which has been found by other investigators at TFSO. The mean and standard deviation of the residuals are 0.95 sec and 0.63 sec, respectively. The elevation correction at TFSO is about 0.25 sec so the anomaly due to the crust and upper mantle is approximately 0.70 sec. This is in good agreement with the value of 0.69 sec which Cleary and Hales (1966) obtained and the value of 0.64 sec which Herrin and Taggart (1968) obtained. In order to simulate the situation at TFSO we have constructed a velocity model that consists of the CIT 208 model below a depth of 150 km and the R and M models of Table 2 above this depth at the source and station, respectively. Travel time residuals for this model are 0.65 sec greater than those shown in Figure 11 for the CIT 208 model with the R upper mantle model at both the source and station. Thus the differences between models M and R is consistent with the *P* delay at TFSO. We must emphasize that only the average velocities of these upper mantle models are well determined quantities, and the particular shape of the velocity variations is somewhat arbitrary.

The amplitudes of seismic waves are especially sensitive to the velocity gradients

near the bottom of their ray paths and therefore provide another check upon velocity models for the mantle. To a good approximation the log of the amplitude is proportional to $\mid d^2T/d\Delta^2 \mid$ which is just the absolute value of the slope of the p curve. Gutenberg and Richter (1956) collected a large amount of observational data on amplitudes in the course of their studies on a magnitude scale for body waves, and Gutenberg made considerable use of this data in constructing his velocity models for the mantle. More recently Vanek and Stelzner (1960) have constructed amplitude-distance curves for European and Asian earthquakes, Carpenter *et al* (1967) has measured the amplitudes of explosions, and Cleary (1967) has measured the amplitudes of earthquakes at U. S. stations. Although the results of all these studies have some features in common, there is still considerable scatter in the observational data.

We have used geometrical ray theory to calculate amplitudes for the CIT 206 and CIT 208 models, and the results are shown in Figure 13 along with the observed amplitudes of Gutenberg and Richter (1956). The results of Gutenberg and Richter are for the vertical component of 1 sec waves from a normal focus earthquake. The agreement
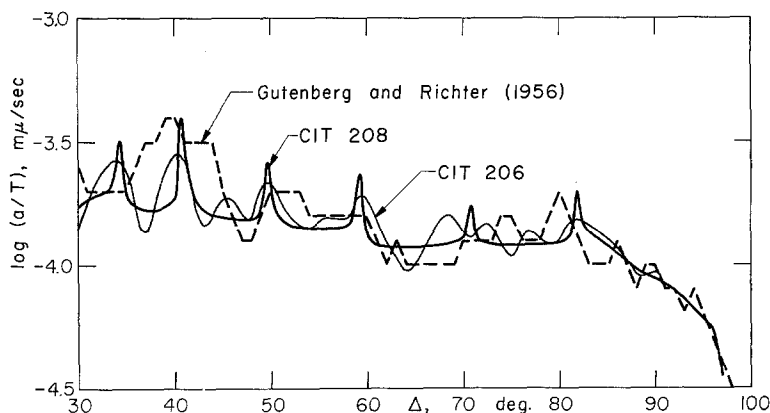
FIG. 13. A comparison of the geometrical spreading terms that were calculated for the CIT 206 and CIT 208 velocity models with the observed amplitudes of Gutenberg and Richter.

between the calculated and observed curves is fair. The maximums near 40 and 50°, the minimum near 65°, the maximum near 80°, and the general decrease beyond 85° are all features that appear to be common to both the observed and calculated curves. However, the amplitude data shown here are not capable of differentiating between the CIT 206 and CIT 208 models. Furthermore, if the observational results of the studies we mentioned above were plotted on the same figure, the matter would become even more ambiguous.

There are numerous explanations for scatter in the observed amplitudes of short-period body waves from earthquakes. The uncertainty in the magnitude, the radiation pattern, variations in the elastic properties of the medium underlying the receiver, attenuation along the path, and scattering due to heterogeneities in the crust and upper mantle near either the source or receiver are just a few of the factors that may contribute to the difficulties in measuring and using amplitude data. In order to avoid some of these problems we have attempted to measure relative changes of amplitudes with distance instead of absolute amplitudes. We have used the array to measure $dA/d\Delta$ (where A is the amplitude) is essentially the same way we measured $dT/d\Delta$. For a given earthquake the trace amplitudes were measured on develicorder film for the maximum motion in the first two cycles of the P wave on all channels of the array. The

periods, T, were also estimated and the ground amplitudes in millimicrons, A, were then obtained by correcting for the magnifications and frequency responses of the various instruments. The quantity $\log(A/T)$ was regarded as a function of distance from the epicenter and fit with a least-squares straight line. The slope of this line was taken as an estimate of $d[\log(A/T)]/d\Delta$.

Measured values of $d[\log(A/T)]/d\Delta$ for 83 of the earthquakes of this study are shown in Figure 14. The calculated values of this quantity for the CIT 206 and CIT 208 models are also shown. The calculated values have been averaged over a window of $2.5°$ in order to simulate the finite size of the array. There appears to be a certain degree of agreement between the observed and calculated values in the distance range of 30 to $50°$. But in general the scatter in the observed data is too large to allow a meaningful comparison with the calculated curves. Our feelings about the future use of $dA/d\Delta$ as a diagnostic aid in the interpretation of mantle velocities are actually more optimistic than the inconclusive results of Figure 14 might indicate. The frequency response and calibration of the instruments were not as well controlled as they should have been
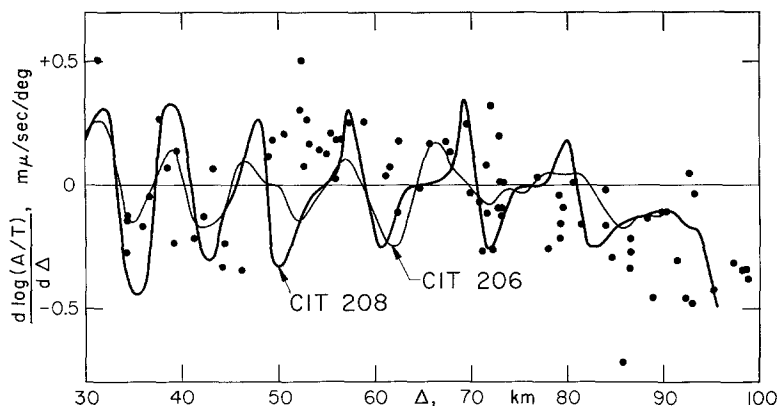
Fig. 14. Measured values of amplitude derivatives and the curves that were calculated for the CIT 206 and CIT 208 velocity models.

for this type of experiment, and this undoubtedly added to the scatter of the results. The advantages of this approach to the amplitude problem appear to be great enough to warrant further investigation of this technique.

THE RADIUS OF THE CORE

The boundary between the mantle and the core is the largest velocity discontinuity in the Earth, and so it is not surprising that the precise location of this boundary has received so much attention by geophysicists. In order to determine the core radius one must first have a velocity model for the entire mantle, and the accuracy of the core radius is closely related to the accuracy of this velocity model. We will briefly review some of the earlier studies of this problem, and this will serve to illustrate some of the problems that are encountered in estimating the core radius.

Gutenberg (1914) was the first to obtain an accurate core radius. His analysis of the direct P waves gave a core radius of 3471 km. Gutenberg and Richter (1935) repeated this analysis with a different set of data and obtained essentially the same results. They took the boundary between the direct P and diffracted P as being $103.5°$ because the amplitudes of short-period P waves decrease rapidly beyond this distance. They then integrated $dT/d\Delta$ obtained from travel-time curves and found that this distance corre-

sponded to a velocity of 13.7 km/sec at a radius of 3451 km. This they took to be the radius of the core, but estimated that its uncertainty was possibly as much as 50 km. They also showed that this velocity and depth were consistent with the apparent velocity of diffracted P waves and the travel times of PcP and ScS waves.

Dahm (1936) on the other hand used different travel-time curves and found the shadow boundary to be at 102.5°. With his velocity model this corresponded to a velocity of 13.42 km/sec at a radius of 3591 km. This depth was not consistent with PcP travel times so he added a layer of decreased velocity and ended up with a velocity of 12.57 km/sec at a core radius of 3371 km (Macalwane, 1951). This decrease in velocity at a radius of about 3600 km has been called the "Dahm discontinuity". Dahm's analysis points out one of the problems encountered when one attempts to measure the core radius. The $dT/d\Delta$ curve begins to flatten beyond a distance of 90° and this indicates that the velocity gradient is beginning to decrease as the core-mantle boundary is approached. Gutenberg (1959, p. 95) actually shows the $dT/d\Delta$ curve as flat in this distance range which implies that the velocity is decreasing at the critical rate $(dv/dr = v/r)$. Should the velocity decrease at a rate larger than this, then it would not be possible to observe the ray which grazes the core. Therefore, because the velocity gradient is small and possibly negative near the core-mantle boundary, it is difficult to obtain an accurate core depth from P waves alone and so one must also use the travel times of PcP and ScS waves.

Jeffreys (1939) inverted his travel-time tables for the direct P and S phases to obtain velocity models for the mantle, and then used the times of PcP and ScS to estimate a core radius of 3473 ± 3 km. His velocity at the bottom of the mantle was 13.64 km/sec.

More recently, several investigators have measured the travel times of PcP from explosions and combined these data with existing velocity models to estimate core radii (Kogan, 1960; Carder, 1964; Buchbinder, 1965). Their estimates of the core radius were all larger than Jeffreys value by amounts of 10 to 30 km.

The most complete set of PcP travel times has been presented by Taggert and Engdahl (1968) who collected the observed PcP times of explosions from a number of studies and applied both station and source corrections to these data. Then they used these data and the velocity model of Herrin et al (1968a) to estimate the core radius. The p curve which was obtained from the travel times of Herrin et al (1968a) shows a pronounced flattening that begins about 90° and the curve reaches a minimum near 99°. However, when the p curve is inverted to obtain a velocity model the ray which emerges at 99° bottoms at a radius of 3565 km, and this is 90 km greater than the accepted core radius. In this sense their results are similar to those of Dahm (1936). Taggert and Engdahl then extrapolated the velocity model downward until they reached a depth which was consistent with the PcP times. The results were a core radius of 3477 ± 2 km, a velocity of 13.67 km/sec at the bottom of the mantle, and a shadow boundary slightly over 99°.

In a slightly different approach, Sacks (1966) measured the amplitudes of short-period P waves and found the shadow boundary to be at a distance of 96 ± 1°. He then used Jeffreys velocity model for P waves and calculated a core radius of 3550 km.

Now let us consider the present study and in particular the CIT 208 velocity model. After corrections were made for the effect of the core, the p values did not show the degree of flattening beyond 90° that has been typical of most studies (see Figure 7). Because of this we did not encounter the type of problem which Dahm (1936) and Taggert and Engdahl (1968) did. We initially took 97° as the shadow boundary and when the data were inverted this distance corresponded to a ray that had penetrated

to a radius of 3491 km. Our next step was to use the observed travel times of *PcP* to estimate the core radius. In Figure 15 we have plotted the Jeffreys-Bullen residuals of the *PcP* travel times given by Taggert and Engdahl (1968). We also grouped these data into 5° intervals and calculated the means and standard deviations that are shown. The velocities of the CIT 208 model were extended downward from the radius of 3491 at a constant velocity in order that *PcP* travel times could be calculated for various trial core radii.

In Figure 15 we have shown the *PcP* travel-time residuals that were calculated for the CIT 208 model with three different trial values of the core radius. The three values of 3479, 3481, and 3483 km have variances of 0.314, 0.270, and 0.317 sec^2, respectively. The value of 3481 is obviously the best of the three estimates. If we assume that the standard deviations that we calculated for the 5° groupings of the data are reasonable estimates of the standard errors of the individual observations, then we can calculate
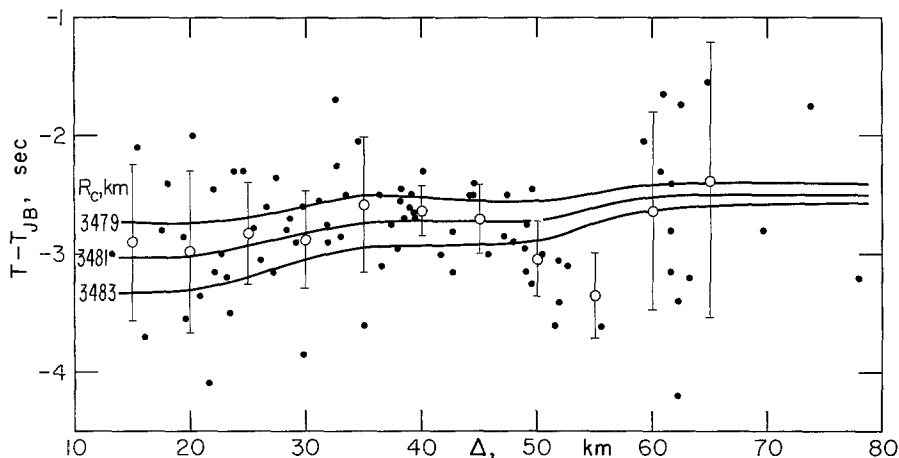
FIG. 15. Travel-time residuals from the Jeffreys-Bullen tables of PcP waves. The points are observed values from explosions that are taken from the paper by Taggert and Engdahl (1968). The open circles and error-bars are the means and standard deviations, respectfully, of the data grouped into 5° intervals. The curves are the residuals that were calculated for the CIT 208 velocity model with three different values of the core radius.

χ^2 for these fits to the *PcP* data. Including only the data up through a distance of 65°, we obtained $\chi^2 = 91$ on 80 degrees of freedom for the radius of 3481 km, which just qualifies as an acceptable fit. However, by eliminating two points near 55° we get $\chi^2 = 81$ on 78 degrees of freedom and this is definitely an acceptable fit. Thus we have concluded that the CIT 208 model with a core radius of 3481 km is consistent with the observed *PcP* data. The values of 3479 and 3483 km for the core radius give χ^2 of 118 and 114, respectively, on 80 degrees of freedom, and neither of these is acceptable.

All of the above calculations were for the CIT 208 velocity model. However, the CIT 206 and CIT 210 curves are equally acceptable fits to the basic *p* data. If we use the same methods to estimate the core radius for these models we find values of 3482 and 3481 km for the CIT 206 and CIT 210 models, respectively. Thus we have estimated the average core radius to be 3481 km with an uncertainty of ±2 km. But we must emphasize the fact that this uncertainty is based only upon the internal consistency of the data of this study, and so the interpretation of this quantity as a measure of the true accuracy of our result is of questionable validity.

VELOCITY ANOMALIES IN THE LOWER MANTLE

The results of this study strongly support the hypothesis that there are definite "anomalies" in the velocities of the lower mantle. That is, there are zones of the lower mantle which have velocity gradients that are appreciably different from the average gradients. These anomalies in the lower mantle are an order of magnitude smaller than those that have been proposed for the upper mantle, and they have a negligible effect upon the travel times. However, if the velocities are used to infer other physical properties of the mantle such as density or composition, then these anomalies are significant.

There are many other studies of seismic data that have indicated the existence of anomalies in the velocities of the lower mantle. We would like to compare the results of these studies with each other and with the results of the present study in order to determine their mutual consistency. So in the next few paragraphs we will briefly review some of the various types of seismic evidence which bear upon this question of anomalies in the lower mantle.

Gutenberg used amplitudes in conjunction with the travel-time data to infer the velocity structure of the mantle. He emphasized the regions with anomalously low velocity gradients. Gutenberg and Richter (1935) found irregularities of this type near depths of about 1000, 1800, and 2300 km. They also found some evidence of reflected waves from this bottom irregularity but the reflection data was more consistent with a depth of about 2400 km. Gutenberg (1958) mentioned only two such low gradient regions, one between depths of 900 and 1000 km and the other between 1400 and 1500 km. Repetti (1928) studied the travel time tables of A. and S. Mohorovicic and found abrupt changes in the apparent surface velocity at distances of 32.2, 39.4, 65, and 77.5°. The resulting velocity model had second order discontinuities at depths of 973, 1140, 1860, and 2100 km. He also identified reflections from the 970 km discontinuity and this particular discontinuity is sometimes referred to as the "Repetti discontinuity". Hoffman et al. (1961) studied the records of quarry blasts and interpreted some of the arrivals to be reflections from a depth of 910 km.

In a study of amplitudes Vvedenskaya and Balakina (1959) found that the ratio of P waves to SH waves and also the ratio of SV waves to SH waves showed anomalously large values near the distances of 38–42°, 51–53°, 70°, and about 80°. They interpreted these results in terms of anisotropy of the mantle velocities at approximate depths of 900–1000 km, 1200–1300 km, 1800 km, and 2200 km. Bugayevskiy (1964) found evidence for first order discontinuities in the travel-time curve near the distances of 35–38°, 50–54°, and 70–72°. The author suggested that these were due to low-velocity zones at depths of about 900, 1200, and 1800 km. Kondorskaya et al (1967) studied the spectra of P waves and plotted the slope of the envelope of the spectra as a function of distance. The results were consistent with discontinuities at distances of 38, 52, and 71°. Mohammadioun (1967) also studied the spectra of P waves and found indications of absorbent (low Q) regions between 650 and 950 km and between 1800 or 2000 and 2900 km.

In their study of $dT/d\Delta$ measured with the LASA array Chinnery and Toksoz (1967) found anomalous features at distances of 35, 52, and 70° which corresponded to anomalously low velocity gradients at depths of approximately 800, 1300, and 2000 km, respectively. In comparing the $dT/d\Delta$ values obtained in their study with those of the present study we find fairly good agreement in some distance ranges and rather large differences in others. The maximum difference is about 0.2 sec/deg near a distance of 65° which results in a maximum difference in the resulting velocity models of about 0.11 km/sec near a depth of 1850 km. Such a comparison between the results of this

study and the one of Chinnery and Toksoz illustrates a problem which is often en-
countered when the results of various studies are compared. Chinnery and Toksoz
interpreted apparent flat portions of the p curve as being anomalous, whereas we have
interpreted apparent steep portions of the p curve as being anomalous. Thus it is not
surprising that the distances and depths associated with these different interpretations
show some disagreement. In order to resolve this problem it will probably be necessary
to combine the p data from several arrays and then analyze it by a method such as that
suggested by Douglas and Corbishley (1968).

Kanamori (1967) used an array in Japan to study $dT/d\Delta$ and found an apparent dis-
continuity at a distance of about 43° which corresponded to an increase in the velocity
gradient at a depth of about 950 km. Archambeau et al (1968) have studied travel
times from nuclear explosions in the western U. S. They find evidence for a change in
slope of the travel time curve near a distance of 41–42° and interpret this in terms of a
high gradient region at a depth of about 1050 km.

The observed amplitude data which we discussed in an earlier section can also be
used as evidence for anomalies in the velocities of the mantle. The fact that the ampli-
tudes show maxima and minima when plotted as a function of distance indicates that
the velocity gradients in the mantle have corresponding maxima and minima.

From the preceding discussion it is clear that there is a considerable body of observa-
tional evidence that supports the existence of anomalous features in the velocities of
the lower mantle. If we consider the common features of the various studies we can
make the generalization that most of the studies have indicated anomalous features in
the epicentral ranges of 35–43, 50–52, and 70–71°. These distances correspond roughly
to the depths of 900–1000, 1200–1300, and 1900–2000 km, respectively. The CIT 208
model also contains anomalous features in these distance and depth ranges.

A disturbing aspect of this consideration of anomalies in the lower mantle is that a
quantitative comparison of the results from the various studies reveals a lack of agree-
ment which is considerably larger than what one would expect from the uncertainties
of the individual studies. Let us briefly examine some of the factors which may con-
tribute to this lack of agreement. Part of the disagreement undoubtedly comes from
the fact that we have compared interpretations of data instead of the actual data itself.
There are at least two reasons why this distinction is important. The first stems from
the fact that the seismological data are observed as a function of time and distance on
the surface of the earth but are interpreted in terms of depth within the earth. Thus a
velocity model has to be introduced in the conversion of distances to depths, and the
resulting depths will depend upon the velocity model which is chosen. We can some-
times avoid this problem by comparing the observed data as a function of distance, but
this is not always possible. The second reason involves the meaning of the word "anom-
aly", and Figure 8 can be used to illustrate this problem. The CIT 208 velocity model
has fairly localized regions with higher than average velocity gradients, and these have
been referred to as "anomalies". The solution to the problem is fairly straightforward
for this model because of the systematic manner in which we fit the p data. But when
we consider the velocity model of Gutenberg the situation is different. This model
definitely has "anomalies" but it is difficult to determine just where the gradients are
average and where they are anomalous. Furthermore, the gradients of some regions are
greater than average and those of others are smaller than average, and so we have
different kinds of anomalies. An associated problem results from the fact that these
anomalies are usually spread out over distances of 50 km or more with indistinct be-
ginnings and endings, and so it is difficult to associate a single depth with them. Note

that the word "discontinuity" has been used by many authors to indicate discontinuities in either the velocities of their derivatives and this is essentially synonymous with our use of the word "anomaly".

Another source of the disagreements among the various results may lie in the inadequacies of the theories which are used in the interpretation of the data. For example, it is questionable whether first-order ray theory is satisfactory for the interpretation of the amplitude data (see for example Červený, 1967). Still another complication which we have not discussed is the possibility of lateral variations in these velocity anomalies (Toksöz et al, 1967).

Although there is still considerable uncertainty about the existence of anomalous velocity gradients in the lower mantle and also about the exact nature of these anomalies if they do exist, it is interesting to speculate about some of the possible implications of these features. In particular, we will consider the implications of the CIT 210 model
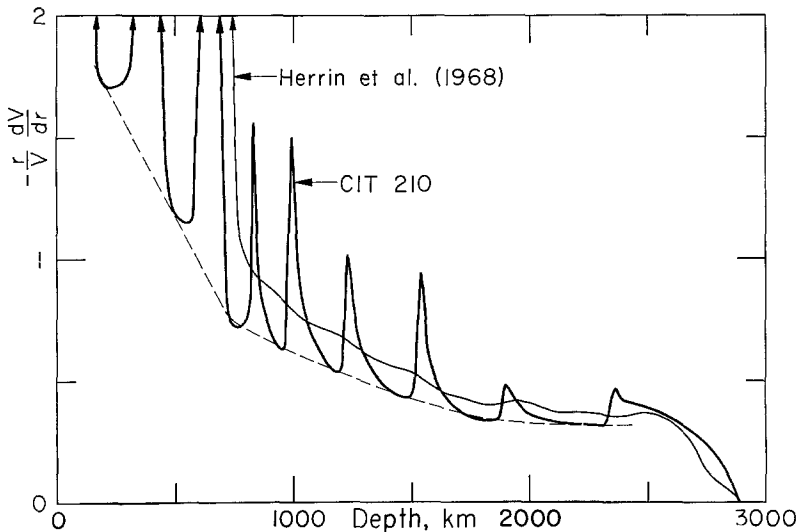
FIG. 16. Gradients of P velocities in the mantle. The dashed curve represents the envelope of the normal gradient regions of the CIT 210 model.

upon the physical state of the lower mantle. The CIT 208 and CIT 210 models are nearly identical except for the fact that the high gradient regions are slightly more localized in the CIT 210 model. In Figure 16 we have plotted the nondimensional velocity gradients of the CIT 210 model as a function of depth. For comparison we have also shown the velocity gradients calculated from the model of Herrin et al. (1968a) which is typical of smooth velocity models with no anomalous features.

The high gradient regions of the CIT 210 model are very conspicuous in Figure 16. The success of Anderson (1967) in explaining the high gradient regions of the upper mantle by means of solid-solid phase changes immediately suggests that similar phenomena might explain these features of the lower mantle. Unfortunately, laboratory experiments have not yet produced results appropriate for these depths so we cannot check this hypothesis at the present time. We have estimated the percentage increase of the velocities within the high gradient regions near the depths of 830, 1000, 1230, 1540, and 1910 km and have obtained values of 0.45, 0.79, 0.59, 0.65, and 0.32 per cent, respectively. The sum total of these five regions represents about 17 per cent of the velocity increase between the depths of 800 and 2300 km. Note that there is also an in-

crease in the velocity gradient near a depth of 2370 km but this increase is not confined to a narrow region.

The existence of the anomalous regions in the CIT 210 model has another indirect implication upon the velocity gradients in the lower mantle. If we focus our attention not upon the high gradient regions but rather upon the intervening "normal" regions, we see that the envelope of these normal regions can be approximated by the smooth curve shown in Figure 16. We can think of the velocity gradients as being composed of this normal curve with the anomalous high gradient regions superposed. Note that throughout most of the mantle there is a systematic difference between this normal curve for the CIT 210 model and the model of Herrin. Thus we see that two models which have very similar average velocities and travel times (see Figures 9 and 11) can yield considerably different estimates of the effects of pressure and temperature on the velocities of the lower mantle.

Figure 16 also provides a useful manner of illustrating some of the general trends of the P velocities in the Earth. Again considering the envelope of the normal regions of the CIT 210 model, we see that the division between the upper and lower mantle becomes quite apparent. The upper mantle is characterized by large rapidly-changing gradients while the lower mantle is characterized by smaller slowly-changing gradients. The approximate boundary between these regions appears to be in the depth range of 700 to 800 km. Other interesting features of this curve are the region between depths of 1800 and 2300 km where the normal velocity gradient is almost constant and the increased gradient between the depths of 2350 and 2650 km. The rapid decrease in the gradient near the core-mantle boundary is also clearly indicated.

CONCLUSIONS

The general objective of this study has been to derive a complete velocity model for the mantle from the measured $dT/d\Delta$ data from one particular array. In the analysis and inversion of this p data we have attempted to be as consistent and as complete as possible so that the resulting model might represent an unbiased estimate of the actual velocities in the Earth. We have explicitly taken account of the correction for the focal depth of the earthquakes, the ellipticity correction, corrections for the crustal structure under each site of the array, the effect of the anomalous upper mantle below the array, the fact that the upper mantle below the source is different from that below the array, and the effect of the core. The resulting velocity model is in good agreement with empirical travel time curves and this serves as an independent check upon both the data and analysis of this study.

With one exception, the effects of azimuth and focal depth upon the p data are fairly small and have a negligible effect upon the final results. The exception consists of earthquakes from the mid-Atlantic ridge which yield anomalously large values of p. The cause of this effect has not been determined, but a block of low velocity material beneath the axis of the ridge appears to be the most promising explanation at the present time.

We have shown that the presence of the core has a significant effect upon the measured p values beyond an epicentral distance of 90°. When this effect is removed from the data the evidence for a complicated velocity structure near the core-mantle boundary is also removed. Empirical PcP times were combined with the velocity model of this study to estimate a core radius of 3481 km.

The velocity model that has emerged from this study is in good agreement with those of other recent studies. A comparison of these various independent estimates of the

mantle velocities suggests that throughout most of the lower mantle the average velocities are now known with an uncertainty of less than 0.05 km/sec.

The data of this study definitely suggest that there are regions of the lower mantle with anomalous velocity gradients. However, when the results of this study are compared with those of other studies it is clear that there is still a considerable degree of uncertainty about the exact nature and location of these anomalous regions. If further studies should confirm the existence of these anomalous features in the elastic velocities, they will serve as additional constraints upon estimates of other physical properties of the mantle.

REFERENCES

Alexander, S. S. and R. A. Phinney (1966). A study of the core-mantle boundary using P waves diffracted by the Earth's core, *J. Geophys. Res.* **71**, 5943–5958.

Anderson, D. L. (1966). Recent evidence concerning the structure and composition of the Earth's mantle, in *Physics and Chemistry of the Earth* **6**, Pergamon Press, New York.

Anderson, D. L. (1967). Phase changes in the upper mantle, *Science* **157**, 1165–1173.

Archambeau, C. B., E. A. Flinn and D. G. Lambert (1969). Fine structure of the upper mantle, *in preparation.*

Birch, F. (1952). Elasticity and constitution of the Earth's interior, *J. Geophys. Res.* **57**, 227–286.

Birch, F. (1961). Composition of the Earth's mantle, *Geophys. J. R. Astr. Soc.* **4**, 295–311.

Birch, F. (1964). Density and composition of mantle and core, *J. Geophys. Res.* **69**, 4377–4388.

Buchbinder, G. G. R. (1965). PcP from the nuclear explosion Bilby September 13, 1963, *Bull. Seism. Soc. Am.* **55**, 441–461.

Bugayevskiy, G. N. (1964). Travel time curve of seismic waves and structure of the mantle, in *Voprosy Seysmichnosti Sibiri, Akad. Nauk SSSR Sibirskoye Otdeleniye, Inst. Zemnoy Kory Trudy* **18**, 151–168.

Bullard, E. C. (1957). The density within the Earth, *Ned. Geol. Mijnbouwk, Genoot. (Geol. Ser.)* **18**, 23–41.

Bullen, K. E. (1963). *Theory of Seismology*, 3rd ed., 381 pp., Cambridge University Press.

Bullen, K. E. and R. A. W. Haddon (1967). Earth models based on compressibility theory, *Phys. Earth Planet. Interiors* **1**, 1–13.

Carder, D. S. (1964). Travel times from central Pacific nuclear explosions and inferred mantle structure, *Bull. Seism. Soc. Am.* **54**, 2271–2294.

Carder, D. S., D. W. Gordon and J. N. Jordan (1966). Analysis of surface-foci travel times, *Bull. Seism. Soc. Am.* **56**, 815–840.

Carpenter, E. W., P. D. Marshall and A. Douglas (1967). The amplitude-distance curve for short period teleseismic P waves, *Geophys. J. R. astr. Soc.* **13**, 61–70.

Červený, V. (1967). The amplitude-distance curves for waves reflected at a plane interface for different frequency ranges, *Geophys. J. R. astr. Soc.* **13**, 187–196.

Chinnery, M. A. and M. N. Toksöz (1967). P-wave velocities in the mantle below 700 km, *Bull. Seism. Soc. Am.* **57**, 199–226.

Cleary, J. (1967). Analysis of the amplitudes of short-period P waves recorded by Long Range Seismic Measurement Stations in the distance range 30° to 102°, *J. Geophys. Res.* **72**, 4705–4712.

Cleary, J. and A. L. Hales (1966). An analysis of the travel times of P waves to North American stations in the distance range 32° to 100°, *Bull. Seism. Soc. Am.* **56**, 467–489.

Dahm, C. G. (1936). Velocities of P waves in the Earth calculated from the Macelwave P curve, 1933, *Bull. Seism. Soc. Am.* **26**, 1–11.

Douglas, A. and D. J. Corbishley (1968). Measurement of dT/dΔ, *Nature* **217**, 1243–1244.

Gogna, M. L. (1967). Travel times from central Pacific nuclear explosions, *Geophys. J. R. astr. Soc.* **13**, 503–527.

Gutenberg, B. (1914). Ueber Erdbebenwellen VII A. Beobachtungen an Registrierungen von Fernbeben in Gottingen und Folgerungen uber die Konstitution des Erdkorpers, *Nachr. Ges. Wiss. Gottingen Math.-physik. Kl.*, 166–218.

Gutenberg, B. (1958). Velocity of seismic waves in the Earth's mantle, *Trans. Am. Geophys. Union* **39**, 86–489.

Gutenberg, B. (1959). *Physics of the Earth's Interior*, 240 pp. Academic Press, New York and London.

Gutenberg, B. and C. F. Richter (1935). On seismic waves II, *Gerlands Beitr. Geophysik* **45**, 280–360.

Gutenberg, B. and C. F. Richter (1956). Magnitude and energy of earthquakes, *Annali di Geofisica* **9**, 1–15.

Hales, A. L., J. R. Cleary and J. L. Roberts (1968). Velocity distribution in the lower mantle, *Bull. Seism. Soc. Am.*, **58**, 1975–1989.

Herrin, E. (ed.), E. P. Arnold, B. A. Bolt, G. E. Clawson, E. R. Engdahl, D. W. Gordon, A. L. Hales, J. L. Lobdell, O. Nuttli, C. Romney, J. Taggart and W. Tucker (1968a). 1968 Seismological tables for P phases, *Bull. Seism. Soc. Am.* **58**, 1193–1241.

Herrin, E., W. Tucker, J. Taggart, D. W. Gordon and J. L. Lobdell (1968b). Estimation of surface focus P travel times, *Bull. Seism. Soc. Am.* **58**, 1273–1291.

Herrin, E. and J. Taggart (1968). Regional variations in P travel times, *Bull. Seism. Soc. Am.* **58**, 1325–1337.

Hoffman, J. P., J. W. Berg and K. L. Cook (1961). Discontinuities in the earth's upper mantle as indicated by reflected seismic energy, *Bull. Seism. Soc. Am.* **51**, 17–27.

Jeffreys, H. (1939). The times of PcP and ScS, *Mon. Not. R. astr. Soc., Geophys. Suppl.* **4**, 537–547.

Jeffreys, H. (1962). Travel times for Pacific explosions, *Geophys. J. R. Astr. Soc.* **7**, 212–219.

Johnson, L. R. (1966). *Measurements of Mantle Velocities of P Waves with a Large Array*, Ph.D. thesis, Calif. Inst. Tech., Pasadena.

Johnson, L. R. (1967a). Measurement of velocities in the mantle with a large seismic array, paper presented at *14th General Assembly of the I. U. G. G.*, Zurich, Switzerland.

Johnson, L. R. (1967b). Array measurements of P velocities in the upper mantle, *J. Geophys. Res.* **72**, 6309–6325.

Kanamori, H. (1967). Upper mantle structure from apparent velocities of P waves recorded at Wakayama Micro-Earthquake Observatory, *Bull. Earthquake Res. Inst. Tokyo Univ.* **45**, 657–678.

Kogan, S. D. (1960). Travel times of longitudinal and transverse waves calculated from data on nuclear explosions made in the region of the Marshall Islands, *Izvestia Akad. Nauk SSSR, Geophys. Ser.* **3**, 371–380.

Kondorskaya, N. V., L. N. Pavlov, A. N. Pustovitenko and S. L. Solov'ev (1967). Some results of a study of the longitudinal wave spectra from earthquakes in the Far East, *Izvestia Akad. Nauk SSSR, Earth Physics* **1**, 60–75.

Macelwane, J. B. (1951). Evidence on the interior of the earth from seismic sources, in *Internal Constitution of the Earth*, B. Gutenberg, ed., 2nd ed., 227–304, Dover, New York.

Mohammadioun, B. (1967). Structure of the earth's mantle and core according to the energy spectra of longitudinal waves, *Annales de Geophysique* **23**, 61–107 .

Niazi, M. and D. L. Anderson (1965). Upper mantle structure of western North America from apparent velocities of P waves, *J. Geophys. Res.* **70**, 4633–4640.

Phinney, R. A. and L. M. Cathles (1968). Diffraction of P by the core: A study of long-period amplitudes near the edge of the shadow, *J. Geophys. Res.* **73**, in press.

Phinney, R. A. and S. S. Alexander (1966). P wave diffraction theory and the structure of the core-mantle boundary, *J. Geophys. Res.* **71**, 5959–5975.

Pilant, W. L. and L. Knopoff (1964). Observations of multiple seismic events, *Bull. Seism. Soc. Am.* **54**, 19–39.

Press, F. (1966). Seismic velocities, in *Handbook of Physical Constants*, S. Clark (ed.), Memoir 97, Geol. Soc. Am., New York.

Repetti, W. C. (1928). *New Values for Some of the Discontinuities in the Earth*, Dissertation, St. Louis University.

Sacks, S. (1966). Diffracted wave studies of the Earth's core, 1. Amplitudes, core size, and rigidity, *J. Geophys. Res.* **71**, 1173–1193.

Scholte, J. G. J. (1956). On seismic waves in a spherical earth, *Koninkl. Ned. Meteorl. Inst. Publ.* 65.

Taggert, J. and E. R. Engdahl (1968). Estimation of PCP travel times and the depth to the core, *Bull. Seism. Soc. Am.* **58**, 1293–1303.

Toksöz, M. N., M. A. Chinnery and D. L. Anderson (1967). Inhomogeneities in the Earth's mantle, *Geophys. J. R. astr. Soc.* **13**, 31–59.

Tryggvason, E. (1961). Wave velocities in the upper mantle below the Arctic-Atlantic Ocean and Northwest Europe, *Annali di Geofisica* **14**, 379–392.

Tryggvason, E. (1964). Arrival times of P waves and upper mantle structure, *Bull. Seism. Soc. Am.* **54**, 727–736.

Vanek, J. and J. Stelzner (1960). The problem of magnitude calibrating functions for body waves, *Annali di Geofisica* **13**, 393–407.

Vvedenskaya, A. V. and L. M. Balakina (1959). Double refraction in the earth's mantle, *Izvestia Akad. Nauk SSSR, Geophys. Ser.* **7**, 1138–1146.

DIVISION OF GEOLOGICAL SCIENCES
CALIFORNIA INSTITUTE OF TECHNOLOGY
PASADENA, CALIFORNIA
CONTRIBUTION NO. 1569.